Title

A mutation in the low-complexity domain of splicing factor hnRNPA1 linked to amyotrophic lateral sclerosis disrupts distinct neuronal RNA splicing networks

Journal

Genes & Development, 38(1-2)

ISSN

0890-9369

Authors

Lee, Yeon J

Rio, Donald C

Publication Date

2024

DOI

10.1101/gad.351104.123

Peer reviewed

A mutation in the low-complexity domain of splicing factor hnRNPA1 linked to amyotrophic lateral sclerosis disrupts distinct neuronal RNA splicing networks

Yeon J. Lee[1,2] and Donald C. Rio[1,2]

[1]Department of Molecular and Cell Biology, University of California, Berkeley, Berkeley, California 94720, USA;
[2]California Institute for Quantitative Biosciences (QB3), University of California, Berkeley, Berkeley, California 94720, USA

Amyotrophic lateral sclerosis (ALS) is a debilitating neurodegenerative disease characterized by loss of motor neurons. Human genetic studies have linked mutations in RNA-binding proteins as causative for this disease. The hnRNPA1 protein, a known pre-mRNA splicing factor, is mutated in some ALS patients. Here, two human cell models were generated to investigate how a mutation in the C-terminal low-complexity domain (LCD) of hnRNPA1 can cause splicing changes of thousands of transcripts that collectively are linked to the DNA damage response, cilium organization, and translation. We show that the hnRNPA1 D262V mutant protein binds to new binding sites on differentially spliced transcripts from genes that are linked to ALS. We demonstrate that this ALS-linked hnRNPA1 mutation alters normal RNA-dependent protein–protein interactions. Furthermore, cells expressing this hnRNPA1 mutant exhibit a cell aggregation phenotype, markedly reduced growth rates, changes in stress granule kinetics, and aberrant growth of neuronal processes. This study provides insight into how a single amino acid mutation in a splicing factor can alter RNA splicing networks of genes linked to ALS.

[*Keywords*: ALS; amyotrophic lateral sclerosis; hnRNPA1; hnRNPA1 D262V mutant; pre-mRNA splicing; irCLIP; TMT-MS]

Supplemental material is available for this article.

Received August 21, 2023; revised version accepted December 14, 2023.

Amyotrophic lateral sclerosis (ALS) is the third most common adult-onset neurodegenerative disorder worldwide. It is generally characterized by progressive paralysis starting at the limbs and ultimately leading to death caused by respiratory failure. There is no cure, and current treatments fail to slow the progression of the disease. It is known that mutations in RNA-binding proteins (RBPs), such as FUS, TIA1, and TDP-43 (TARDBP) are linked genetically to ALS (Kwiatkowski et al. 2009; Vance et al. 2009; Kim et al. 2013; Johnson et al. 2014; Mackenzie et al. 2017). In addition, mutations in heterogeneous nuclear ribonucleoproteins (hnRNPs; e.g., hnRNPA1 and hnRNPA2/B1) have been linked to familial cases of ALS (Kim et al. 2013; Liu et al. 2016; Beijer et al. 2021; Milicevic et al. 2022). Repeat expansions in the C9orf72 gene also cause ALS and are associated with the formation of RNA foci containing low-solubility hnRNP proteins, suggesting that RNA toxicity via the sequestration of RBPs plays a role in the disease (Cooper-Knock et al. 2014; Conlon and Manley 2017; Balendra and Isaacs 2018; Milicevic et al. 2022). It is becoming evident that mutations in genes encoding RNA-binding proteins are critical determinants of neurological diseases, especially motor neuron disorders such as ALS (Milicevic et al. 2022).

The RNA-binding splicing factor hnRNPA1 contains two RRM-type RNA-binding domains at the N terminus and glycine–arginine-rich and prion-like low-complexity domains at the C terminus. Single-point mutations within this C-terminal domain have been associated with the neurodegenerative disease ALS. There are four known ALS-associated mutations found in the C-terminal domain of hnRNPA1 (Liu et al. 2016; Beijer et al. 2021). The aspartic acid (D)-to-valine (V) mutation at position 262 (D262V) is the only disease-associated variant that impacts an evolutionarily conserved residue in ALS patients (Kim et al. 2013).

Here, we focused on testing the effects of this mutation in hnRNPA1 using genome editing and expression of this mutant protein on global pre-mRNA splicing patterns, target RNA binding, and phenotypic characterization in two human cell line models. Either expression of hnRNPA1 D262V in 293 HEK cells or genome editing the D262V mutation into the endogenous locus in

Corresponding author: don_rio@berkeley.edu
Article published online ahead of print. Article and publication date are online at http://www.genesdev.org/cgi/doi/10.1101/gad.351104.123. Freely available online through the *Genes & Development* Open Access option.

neuronal SH-SY5Y cells led to marked changes in the patterns of RNA splicing of thousands of transcripts, some being linked to the DNA damage response and cilium organization. The splicing pattern changes due to the hnRNPA1 mutation also affected transcripts for other RNA-binding proteins linked to ALS, such as MATR3, TDP-43, FUS, and ATXN2. In order to determine whether these differential splicing events were generated by binding of the hnRNPA1 D262V mutant protein to a different subset of pre-mRNAs compared with wild-type hnRNPA1, we performed infrared CLIP (irCLIP) experiments for efficient characterization of in vivo protein–RNA interactions. In many cases, the splicing pattern changes could be linked to alterations in binding of the wild-type or mutant hnRNPA1 protein to splicing target transcripts.

Phenotypically, expression of the hnRNPA1 D262V mutant protein caused the cells to clump together and aggregate, resulting in a marked reduction in cell growth rate and changes in stress granule disassembly dynamics. This behavior might explain, in part, the neuronal cell death caused by this mutation in ALS patients. We also differentiated SH-SY5Y cells expressing the hnRNPA1 D262V mutation into mature neurons and found that the mutant cells display defects in neuronal projections and connections, cell aggregation, and slower growth rates. RNA-seq data generated from differentiated SH-SY5Y cells indicated elevated intron retention and composite modes of splicing events in the differentiated hnRNPA1 D262V neuronal cells, an intriguing observation that was not observed in undifferentiated hnRNPA1 D262V cells.

To gain insight into how hnRNPA1 function might be altered by the ALS-associated D262V mutation, we compared hnRNPA1 protein interactomes in wild-type and mutant cells. We used mass spectrometry to identify differentially interacting proteins between the two cell lines. Some of the hnRNPA1 binding partners that we identified were found to be other ALS-linked RNA-binding proteins, such as MATR3, TDP-43, and FUS. In addition, we also found a protein, prohibitin 1, that is linked to both nuclear TP53 function and mitochondrial function. In summary, we present data showing that a single-nucleotide mutation within the low-complexity domain of hnRNPA1 results in significant changes in global pre-mRNA splicing patterns and many RNA–protein interactions. Cells harboring this single amino acid change exhibit phenotypes of slow growth rates, changes in cell–cell interactions, and alteration of neuronal processes upon cell differentiation to neurons. Overall, this study provides further insights into how inherited mutations in the hnRNPA1 gene lead to RNA processing defects that contribute to loss of motor neurons in ALS.

Results

Expression of the hnRNPA1 D262V mutant protein in HEK293 cells and characterization of global RNA pre-mRNA splicing patterns

hnRNPA1 plays an important role in RNA metabolism, including transcription, splicing, nuclear export, translation, and turnover (Jean-Philippe et al. 2013). To test the effects of the hnRNPA1 D262V ALS mutation on RNA processing, our initial approach was to generate inducible cell lines to express either hnRNPA1 wild-type or D262V mutant epitope-tagged cDNAs. This experimental setup was initially designed to mimic ALS patients carrying a heterozygous hnRNPA1 D262V mutation. FLP-In-293 cells expressing hnRNPA1 wild-type or D262V mutant epitope-tagged cDNAs were induced to confirm the induction of the exogenous epitope-tagged hnRNPA1 proteins (Supplemental Fig. S1A). To examine the effect of the hnRNPA1 D262V mutant on global pre-mRNA splicing patterns, we generated RNA-seq libraries from the FLP-In-293 cells expressing either epitope-tagged hnRNPA1 wild-type or mutant proteins. Quantitative alternative splicing (AS) analysis was performed using JUM (junction usage model) software (Lee et al. 2018; Wang and Rio 2018) to detect differential splicing events between the wild-type and D262V mutant cells. JUM is a computational method for quantitating and comparing pre-mRNA splicing patterns from RNA-seq data sets. This analysis resulted in a quantitative comparison of AS events (2240) whose splicing patterns were significantly altered upon expression of Tet-inducible FLP-In hnRNPA1 D262V protein versus the wild-type hnRNPA1 control, covering 1532 genes (Supplemental Fig. S1B). Gene ontology (GO) term enrichment analysis of high-confidence hnRNPA1 D262V mutant splicing targets in 293 cells revealed that these differentially spliced target RNAs are involved in homologous recombination, DNA repair, cilium assembly, cellular response to DNA damage stimuli, and chromatin organization (Supplemental Fig. S1C). Notably, differential gene expression analysis comparing FLP-In-293 hnRNPA1 D262V with wild type revealed only 345 genes whose expression is changed (Supplemental Fig. S2; Supplemental Table S3). These differentially expressed genes are involved in guanine metabolic processes, protein targeting to ER, protein localization to membranes, and SRP-dependent cotranslational protein targeting to membranes (Supplemental Fig. S2; Supplemental Table S3).

Effects of expressing the hnRNPA1 D262V mutation from the endogenous locus in genome-edited human SH-SY5Y neuronal cells

In order to test the effects of expression of the hnRNPA1 D262V mutant protein in human neuronal cells, we used genome editing at the endogenous hnRNPA1 locus in SH-SY5Y human neuroblastoma cells. This approach allowed us to generate both heterozygous and homozygous hnRNPA1 mutant cell lines using Cas9–RNP genome editing. We generated RNA-seq libraries from SH-SY5Y cells expressing either the unedited control hnRNPA1 locus or the genome-edited homozygous hnRNPA1 D262V mutant genes. Although ALS patients are heterozygous for this mutation, using homozygous D262V mutant cells lines for this initial study can provide a clearer picture of the effects of the mutation compared with the heterozygous mutant cell line. We performed JUM bioinformatic analysis to determine changes in pre-mRNA splicing

patterns, comparing the edited cells carrying the hnRNPA1 D262V mutation with the unedited control cells. This analysis resulted in a quantitative comparison of AS events (4368) whose splicing patterns were significantly altered upon expression of the hnRNPA1 mutant D262V protein versus the wild-type control, covering 3322 genes (Fig. 1A). All categories of splicing patterns were affected. GO term enrichment analysis of 3322 differentially spliced (DS) transcripts against 11,394 expressed genes in SH-SY5Y cells indicated that genes with altered splicing patterns were involved in cellular metabolic processes, cilium organization, chromatin remodeling, DNA repair, and cytoskeleton organization (Fig. 1B). The GO term analysis suggests that cellular metabolic or DNA damage stress might result from the splicing alterations caused by expression of the hnRNPA1 D262V mutant protein. We also performed differential gene expression analysis comparing SH-SY5Y hnRNPA1 D262V with unedited control cells, which revealed that only 619 genes are differently expressed (Supplemental Fig. S3; Supplemental Table S4). The GO terminology of differentially expressed genes indicates that these genes are involved in centrosome localization, microtubule-organizing center localization, and gene silencing by miRNA (Supplemental Fig. S3A; Supplemental Table S4). It is known that the molecular pathways disrupted in ALS involve mitochondrial dysfunction, oxidative stress, axonal transport dysregulation, glutamate excitotoxicity, endosomal and vesicular transport impairment, impaired protein homeostasis, and aberrant RNA metabolism (Chen et al. 2013; Madabhushi et al. 2014; Hardiman et al. 2017; Le Gall et al. 2020). Our RNA-seq analysis revealed that the majority of genes that undergo differential alternative splicing and expression in D262V-expressing cells are involved in the aforementioned cellular pathways that are found to be defective in ALS patients.

We compared differential splicing events in FLP-In-293 cells and SH-SY5Y cells expressing the ALS-associated hnRNPA1 D262V mutant protein. A Venn diagram (Fig. 2A) shows that the overlapping DS target RNAs resulting from the two different cell lines expressing the hnRNPA1 D262V mutant resulted in 639 high-confidence splicing targets that were detected by JUM analysis. These high-confidence splicing targets are involved in DNA repair, cellular response to DNA damage stimuli, cellular metabolic processes, chromatin remodeling, and cilium organization and assembly (Fig. 2B). These defective cellular pathways have been in implicated in neurodegenerative diseases (Chen et al. 2013; Madabhushi et al. 2014; Hardiman et al. 2017).

We also searched our data sets to ask whether transcripts encoding known neurodegenerative disease-associated proteins are differentially spliced in cells expressing the hnRNPA1 mutant protein (Table 1). We found many transcripts encoding ALS-linked proteins, including cytoskeletal proteins, RNA-binding proteins, and proteins involved in translation control and proteostasis, that are alternatively spliced in hnRNPA1 D262V-expressing cells, including TARDBP (TDP-43) (Table 1). It is known that expression of mutant or nuclear depletion of TDP-43 results in the alternative splicing of hnRNPA1 transcripts, resulting in expression of an aggregation-prone isoform of hnRNPA1, which could contribute to the disease manifestation in ALS (Deshaies et al. 2018; Sivakumar et al. 2018). Additionally, knockdown of TDP-43 results in increased inclusion of a cassette exon in the hnRNPA1 transcript, yielding an aggregation-prone variant in HeLa cells (Deshaies et al. 2018). Indeed, expression of the hnRNPA1 D262V mutation in SH-SY5Y cells resulted in the elevated inclusion of exon 8 and a more aggregation-prone isoform of the protein (see below; Supplemental Fig. S5).

Given the connection between TDP-43 and hnRNPA1, we wanted to determine whether there is an overlap between differential splicing targets from a TDP-43 knockdown or the ALS-associated TDP-43 N352S mutant (from publicly available data sets) and either an hnRNPA1 knockdown (Supplemental Fig. S6; Lee et al. 2018) or the hnRNPA1 D262V mutant (Supplemental Fig. S7). Differential splicing analysis was performed using JUM, and differential splicing targets were compared. We found ~30%–35% overlap in differentially spliced transcripts for TDP-43 and hnRNPA1. This indicates that TDP-43 and hnRNPA1 are involved in coregulation and share many splicing targets but also clearly have distinct splicing targets from each other. The 593 common splicing targets of hnRNPA1 and TDP-43 in the knockdown experiments were involved in regulation of cellular response to stress, protoporphyrinogen IX biosynthetic process, and histone modification (Supplemental Fig. S6). Our GO term analysis of 593 common splicing targets of hnRNPA1 and TDP-43 suggests that the genes involved in stress response and DNA repair are alternatively spliced and may contribute to the disease development.

We also compared differentially spliced transcripts in the ALS-associated TDP-43 N352S mutant and hnRNPA1 D262V mutant SH-SY5Y cell backgrounds (Supplemental Fig. S7). Again, splicing analysis of RNA-seq data indicated that the two distinct ALS-associated mutants shared some splicing targets but also have distinct splicing targets from each other. Five-hundred-seventy-seven common genes encode transcripts that are differentially spliced in both mutant cells and are involved in cellular component organization, synaptic vesicle budding, regulation of cilium assembly, and regulation of DNA repair (Supplemental Fig. S7). Impaired DNA repair, axonal transport, and ciliary defects, as well as altered RNA metabolism, are all known pathological symptoms of ALS (Mejzini et al. 2019; Wang et al. 2021). Alternative splicing of genes that are involved in these pathways can also contribute to the neuronal loss observed in ALS and perhaps other neurodegenerative diseases. Defects in cilium formation, function, and signaling for neuronal survival are caused by familial mutations in Parkinson's disease (Khan et al. 2021).

Our analysis also shows that differential gene expression profiling found that only 619 genes were differentially expressed in endogenously edited hnRNPA1 D262V SH-SY5Y cells and only 345 genes were differentially expressed in FLP-In-293 cells expressing the D262V mutant, yet there were thousands of differentially

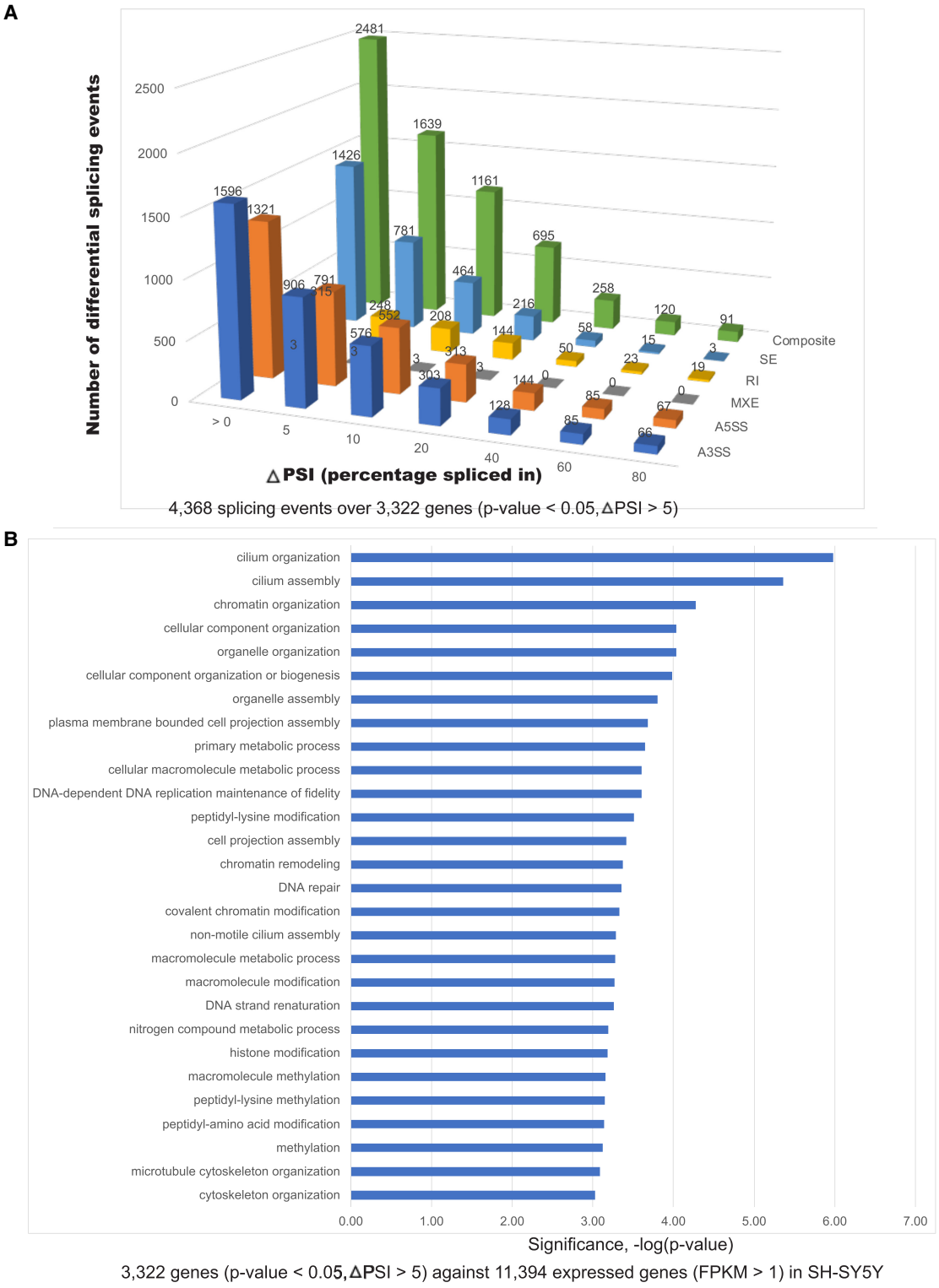

Figure 1. Differential splicing events detected in genome-edited SH-SY5Y neuroblastoma cells expressing the ALS-associated hnRNPA1 D262V mutation. (*A*) Differential alternative splicing (AS) events detected upon expression of the ALS-associated hnRNPA1 D262V mutation. Over 4000 splicing events were significantly altered in hnRNPA1 D262V samples in the neuronal cell line versus the control ($P < 0.05$, $\Delta PSI > 5$). The number of differential splicing events is shown on the *Y*-axis, and the difference in percentage spliced in (PSI) is shown on the *X*-axis. The splicing events were filtered based on the ΔPSI. Types of splicing patterns are indicated at the *right*. (*B*) A graph of gene ontology (GO) term enrichment of differentially spliced transcripts in hnRNPA1 D262V mutant protein-expressing SH-SY5Y cells. These groupings correspond to 3322 genes whose splicing pattern is altered in the mutant cells.

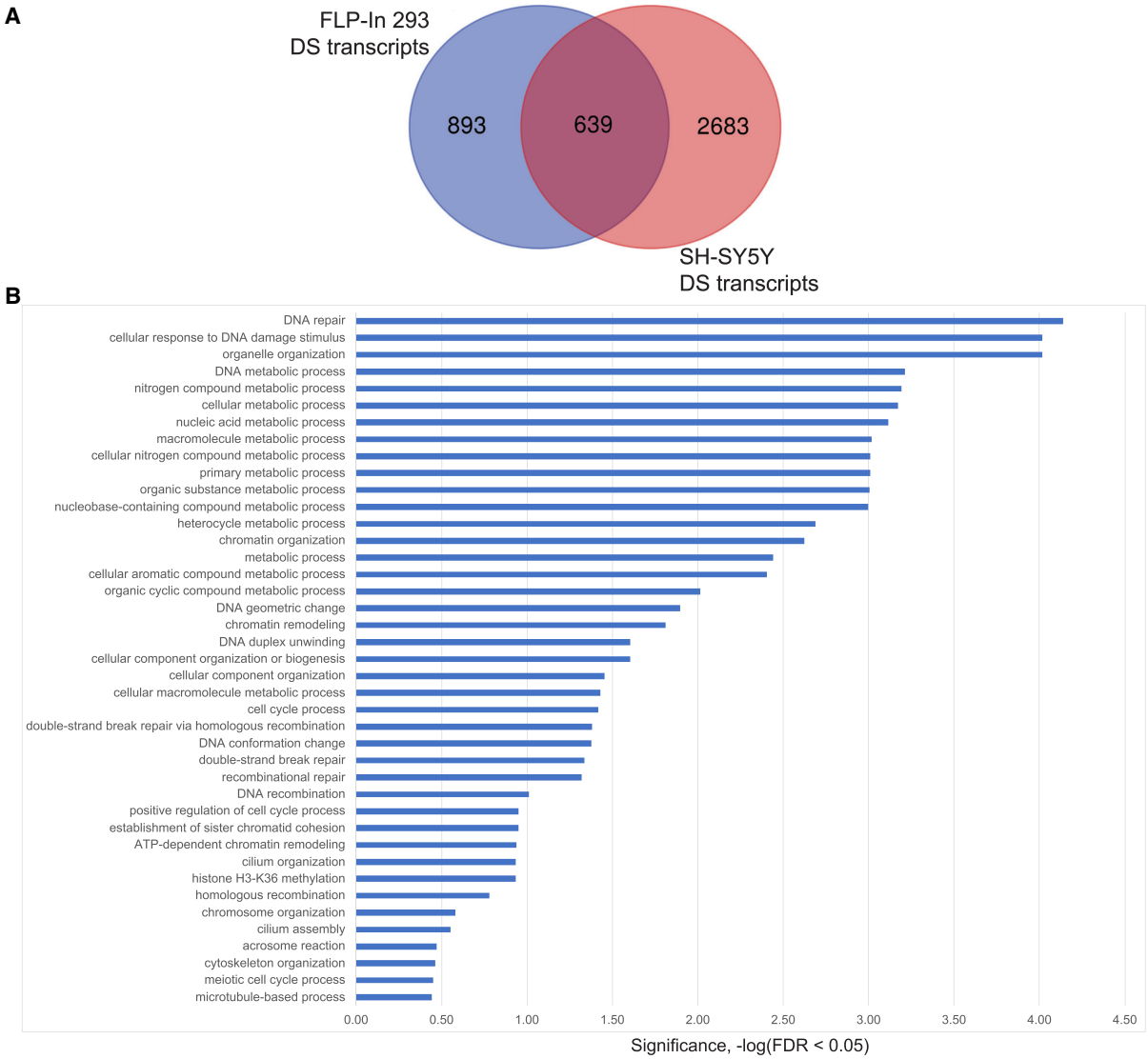

Figure 2. Comparison of differentially spliced (DS) transcripts in FLP-In-293 and SH-SY5Y cells expressing the ALS-associated hnRNPA1 D262V mutation. (*A*) Venn diagram showing the overlapping splicing targets resulting from the FLP-In-293 (blue) and SH-SY5Y (red) cells expressing hnRNPA1 mutant proteins, resulting in 639 high-confidence splicing targets that were detected by JUM. (*B*) A graph of gene ontology (GO) term enrichment analysis of hnRNPA1 D262V mutant splicing targets was performed against all expressed genes in FLP-In-293 cells and in SH-SY5Y neuroblastoma cells. The enriched GO term categories included response to DNA damage stimuli, DNA repair, and cilium assembly that includes cytoskeletal proteins.

spliced transcripts. Thus, importantly, there was minimal overlap between differentially expressed genes versus genes that undergo alternative splicing in hnRNPA1 D262V mutant-expressing cells (Supplemental Figs. S2B, S3B). Our differential gene expression profiling analysis indicated that the glutaminase (GLS) gene is up-regulated in hnRNPA1 D262V-expressing SH-SY5Y neuronal cells compared with the wild-type control (Supplemental Table S4; Supplemental Fig. S3C). Since glutaminase is essential for neuronal cell survival and differentiation, we examined the steady-state expression of GLS protein in both hnRNPA1 D262V mutant and wild-type cells by immunoblotting. We unexpectedly observed a reduced expression of GLS protein only in the hnRNPA1 D262V samples in mild lysis buffer (0.5% n-dodecyl-b-D-maltoside, 150 mM NaCl, 50 mM HEPES-NaOH at pH 7.4), normalized to the total protein expression level (Supplemental Fig. S3D). This made us speculate whether cells expressing hnRNPA1 D262V mutant proteins have a different solubility compared with hnRNPA1 wild type, since only soluble fractions were loaded on gels for the immunoblot analysis. Total protein staining of equal amounts of lysate (15 µg) showed slightly different staining patterns between lysates prepared from hnRNPA1 wild-type and D262V mutant cells in mild lysis buffer (Supplemental Fig. S3D). We next tested GLS protein levels using strong lysis buffer containing 2% SDS in 20 mM HEPES (pH 8.0) and observed a similar level of GLS expression in wild-type

Table 1. *Neurodegenerative disease-associated proteins are identified as high-confidence splicing targets in both SH-SY5Y cells and FLP-In T-REx-293 hnRNPA1 D262V-expressing cells*

	FLP-In-293	SH-SY5Y	Function
VCP	Y		Facilitates autophagy This gene encodes a member of the AAA ATPase family of proteins. The encoded protein plays a role in protein degradation, intracellular membrane fusion, DNA repair and replication, regulation of the cell cycle, and activation of the NF-κB pathway.
VAPB	Y		Facilitates unfolded protein response in protein quality control and may be involved in vesicle trafficking
FUS		Y	DNA/RNA homeostasis This gene encodes a multifunctional protein component of the heterogeneous nuclear ribonucleoprotein (hnRNP) complex. The hnRNP complex is involved in pre-mRNA splicing and the export of fully processed mRNA to the cytoplasm. This protein belongs to the FET family of RNA-binding proteins, which has been implicated in cellular processes that include regulation of gene expression, maintenance of genomic integrity, and mRNA/microRNA processing. Alternative splicing results in multiple transcript variants.
ATXN2	Y	Y	Localizes to the endoplasmic reticulum and plasma membrane, is involved in endocytosis, modulates mTOR signals, and modifies ribosomal translation and mitochondrial function
TIAL-1	Y	Y	Cytotoxic granule-associated RNA-binding protein-like 1; RNA-binding protein; possesses nucleolytic activity against cytotoxic lymphocyte target cells; may be involved in apoptosis
EIF3D	Y		mRNA cap-binding component of the eukaryotic translation initiation factor 3 (eIF-3) complex
EIF4G1	Y	Y	Involved in the recognition of the mRNA cap, ATP-dependent unwinding of the 5′-terminal secondary structure, and recruitment of mRNA to the ribosome
EIF4G2	Y		Binds mRNA cap structure to ribosome; also interacts with the poly(A)-binding protein (PABPx) and increases its RNA-binding activity
EIF4G3	Y	Y	Involved in the recognition of the mRNA cap, ATP-dependent unwinding of the 5′-terminal secondary structure, and recruitment of mRNA to the ribosome
ALS2		Y	A modulator of endocytosis The protein encoded by this gene contains an ATS1/RCC1-like domain, a RhoGEF domain, and a vacuolar protein-sorting 9 (VPS9) domain, all of which are guanine nucleotide exchange factors that activate members of the Ras superfamily of GTPases. The protein functions as a guanine nucleotide exchange factor for the small GTPase RAB5. The protein localizes with RAB5 on early endosomal compartments and functions as a modulator for endosomal dynamics. Mutations in this gene result in several forms of juvenile lateral sclerosis and infantile-onset ascending spastic paralysis. Multiple transcript variants encoding different isoforms have been found for this gene.
SETX	Y		RNA/DNA helicase; role in transcription regulation, mRNA splicing efficiency, and splice site selection This gene encodes a protein named for its homology with the Sen1p protein of fungi, which has RNA helicase activity encoded by a domain at the C-terminal end of the protein. The protein encoded by this gene contains a DNA/RNA helicase domain at its C-terminal end, which suggests that it may be involved in both DNA and RNA processing. Mutations in this gene have been associated with ataxia–ocular apraxia-2 (AOA2) and an autosomal dominant form of juvenile amyotrophic lateral sclerosis (ALS4).
DCTN1		Y	Cytoskeleton dynamics and vesicle traffic This gene encodes the largest subunit of dynactin, a macromolecular complex consisting of 10–11 subunits ranging in size from 22 to 150 kDa. Dynactin binds to both microtubules and cytoplasmic dynein. Dynactin is involved in a diverse array of cellular functions, including ER-to-Golgi transport, the centripetal movement of lysosomes and endosomes, spindle formation, chromosome movement, nuclear positioning, and axonogenesis.
DCTN2	Y		Cytoskeleton dynamics and vesicle traffic This gene encodes a 50-kDa subunit of dynactin, a macromolecular complex consisting of 10–11 subunits ranging in size from 22 to 150 kDa. Dynactin binds to both microtubules and cytoplasmic dynein. Dynactin is involved in a diverse array of cellular functions, including ER-to-Golgi transport, the centripetal movement of lysosomes and endosomes, spindle formation, chromosome movement, nuclear positioning, and axonogenesis.
MATR3	Y	Y	Role in transcription, nuclear retention of defective RNAs, and RNA/DNA homeostasis

Gene names are indicated in the left column. The middle columns indicate whether a splicing pattern change is detected (indicated by Y) from transcripts from the indicated genes from either SH-SY-5Y cells or FLP-In T-REx-293 cells. The right column indicates gene function and the cellular process(es) with which they are involved.

and D262V mutant-expressing cells (Supplemental Fig. S3D). This result confirmed our speculation of differential solubility of D262V mutant protein compared with the wild type and that the GLS protein remains in the insoluble fraction in mild lysis buffer. Hence, it will be important to follow up this observation with insolubility tests for hnRNPA1 D262V cells using lysis buffers with different stringencies. Reduced solubility as well as increased aggregation are related to several neurodegenerative diseases, and here we show that hnRNPA1 D262V expression alone leads to reduced solubility in mild lysis buffer compared with the wild type.

Expression of the hnRNPA1 D262V mutant in either FLP-In-293 or SH-SY5Y cells causes cell aggregation, a markedly reduced growth rate, and a reduction of neuronal processes and connections in differentiated SH-SY5Y cells

We observed a cell aggregation phenotype of hnRNPA1 mutant cell lines in both in FLP-In-293 and SH-SY5Y cells compared with wild type, as well as markedly slower growth rates. Cells expressing the hnRNPA1 D262V mutant protein displayed a distinct cell aggregation phenotype in the FLP-In-293 cells (Supplemental Fig. S8A). We also noted that the FLP-In-293 hnRNPA1 D262V mutant-expressing cells had a slower growth rate compared with the wild-type cells (Supplemental Fig. S8B). This growth inhibition might be related to the neuronal cell death observed in ALS patients.

SH-SY5Y cells have been used increasingly to study neurodegenerative diseases, such as Alzheimer's (Agholme et al. 2010) and Parkinson's disease (Xie et al. 2010). Fully differentiated SH-SY5Y cells express markers of mature neurons, including growth-associated protein (GAP-43), neuronal nuclei (NeuN), synaptophysin (SYN), synaptic vesicle protein II (SV2), neuron-specific enolase (NSE), and microtubule-associated protein (MAP) (Påhlman et al. 1984; Gimenez-Cassina et al. 2006; Agholme et al. 2010). In order to examine whether the growth defects seen in FLP-In-293 D262V cells can also be observed in differentiated neurons, both homozygous and heterozygous hnRNPA1 mutant SH-SY5Y cells were differentiated into mature adherent neurons following a published protocol (Shipley et al. 2016).

A similar growth defect phenotype was observed in genome-edited SH-SY5Y cells expressing both the homozygous and heterozygous hnRNPA1 D262V mutant gene (Fig. 3A). There was a dramatic difference in cell growth rate between SH-SY5Y cells expressing either the hnRNPA1 wild-type or D262V mutant proteins. The cell aggregation phenotype observed in the D262V mutant-expressing 293 cells was also observed in SH-SY5Y cells expressing the hnRNPA1 D262V mutant protein compared with the wild type (Fig. 3B; quantitated in Supplemental Fig. S18). Most interestingly, we observed that the neuronal processes and cell–cell connections characteristic of differentiated SH-SY5Y cells were not as intricate or extensive in the hnRNPA1 mutant D262V cells (both homozygous and heterozygous) compared with wild type in differentiated neurons (Fig. 3C; Supplemental Fig. S19). Taken together, these data show that expression of the hnRNPA1 D262V mutant leads to changes in cell–cell contacts, a marked reduction in cell growth rate, and defects in branching out and connection of neuronal processes characteristic of mature neurons.

In order to determine whether hnRNPA1 D262V could modulate splicing of different subsets of genes following neuronal differentiation, we generated RNA-seq libraries from wild-type and edited hnRNPA1 D262V SH-SY5Y neuronal cells after differentiation. The differentiated neuronal cells expressing both the homozygous and heterozygous hnRNPA1 D262V mutant alleles were harvested and RNA was prepared into RNA-seq libraries and sequenced. RNA-seq data were analyzed for both alternative splicing patterns using JUM and for differential expression profiling using DESeq2. Both heterozygous and homozygous cells expressing hnRNPA1 D262V mutant cells that were differentiated into neurons showed numerous splicing pattern changes, with elevated intron retention and composite modes of splicing events as the most prevalent splicing pattern in differentiated hnRNPA1 D262V neuronal cells compared with wild-type cells (Fig. 4A; Supplemental Fig. S4). Intron retention is the least common human splicing pattern. This is an intriguing observation that was not observed in undifferentiated hnRNPA1 D262V SH-SY5Y cells. For both the homozygous and heterozygous cells, GO term enrichment analysis of alternatively spliced transcripts indicated that these genes are involved in the regulation of cell projections and axonogenesis (homozygous shown in Fig. 4; heterozygous shown in Supplemental Fig. S4). The intron-retained transcripts showed GO term enrichment in metabolism (homozygous shown in Fig. 4) and in cell projections (heterozygous shown in Supplemental Fig. S4). Differential splicing of transcripts from these genes could lead to metabolic alterations and changes in neuronal connectivity that could drive the progressive loss of neurons leading to ALS. Notably, elevated intron retention was also observed in ALS patient biopsy RNA-seq data from C9orf72 samples (Wang et al. 2020).

We compared our data from the differentiated SH-SY5Y cells with ALS C9orf72 patient biopsy samples (Wang et al. 2020); in both cases, elevated intron retention was observed (Supplemental Fig. S20). We observed that ~25% of genes that are differentially spliced overlap between the differentiated SH-SY5Y cells and the C9orf72 patient biopsy sample, and the GO terms for the 705 common genes are involved in synapse organization, microtubule nucleation, regulation of potassium ion transport, and regulation of GTPase activity. The regulation of GTPase activity by GTPase-activating proteins (GAPs) triggers a series of signaling changes, specifically in cell growth, proliferation, and cell death. Increasing evidence supports a role for Rho GTPases in various neurodegenerative diseases (DeGeer and Lamarche-Vane 2013; Stankiewicz and Linseman 2014). Our data also indicate that the transcripts involved in regulation of GTPases are shown to be differentially spliced in the differentiated SH-SY5Y cells and also in the C9orf72 patient biopsy samples, possibly altering the downstream cellular process.

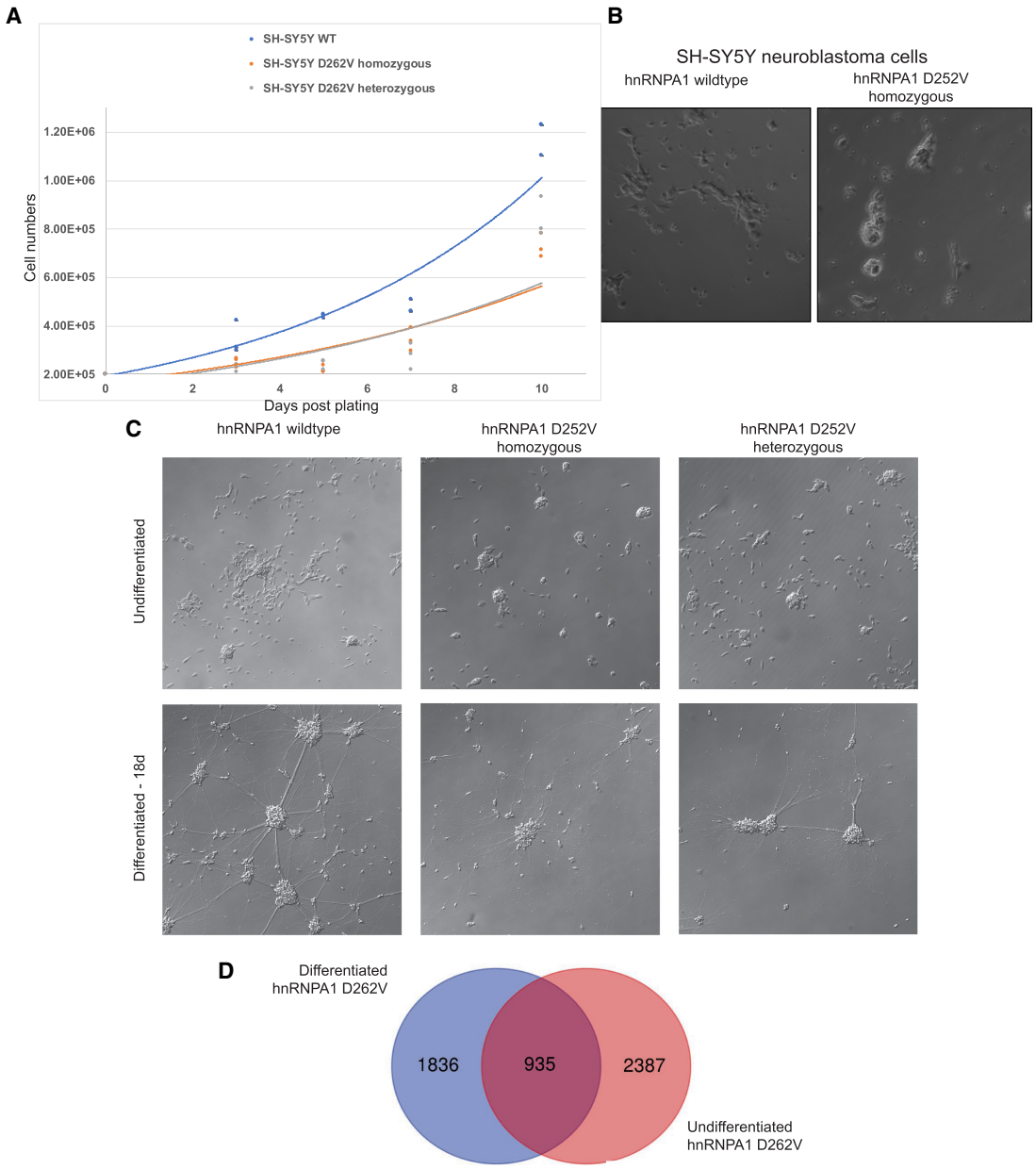

Figure 3. hnRNPA1 D262V mutant SH-SY5Y cells exhibit distinct cell phenotypes, including cell–cell aggregation, slow growth rate, and aberrant formation of neuronal processes. (*A*) Growth curve of SH-SY5Y hnRNPA1 wild-type and edited hnRNPA1 D262V mutant cells. Both homozygous and heterozygous SH-SY5Y hnRNPA1 D262V mutant cells exhibited slower growth rates in comparison with wild type. (*B*) Phase contrast imaging on a confocal microscope of SH-SY5Y undifferentiated cells expressing either hnRNPA1 wild-type (*left* panel) or homozygous hnRNPA1 D262V mutant (*right* panel) proteins. Note that a cell–cell aggregation phenotype is observed for the mutant-expressing cells. (*C*) DIC images of cells that are either undifferentiated (*top* panels) or differentiated (*bottom* panels) for the unedited wild-type control, along with homozygous and heterozygous hnRNPA1 D262V mutant cell lines. Note that both the homozygous and heterozygous D262V mutant cells display slower growth rates and are defective for extension of neuronal processes compared with the wild-type cells. (*D*) Venn diagram showing the overlapping 935 splicing targets that were detected in both undifferentiated and differentiated homozygous hnRNPA1 D262V mutant SH-SY5Y cells.

The hnRNPA1 D262V mutant cells exhibit defects in stress granule disassembly

Recent studies suggest that the response of RNA metabolism to stress plays an important role in neurodegenerative diseases (Nussbacher et al. 2019; Wolozin and Ivanov 2019; Dudman and Qi 2020). RNA-binding proteins (RBPs) control the processing and utilization of mRNAs during stress, in part through formation of stress granules (SGs). SGs are supposed to be transient

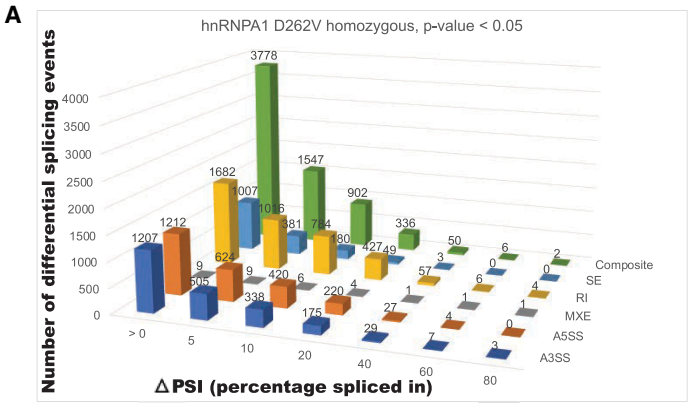

Differentiated for 18d

D262V homozygous mutant, p-value < 0.05, ΔPSI > 5		
PSI > 5	Events	geneID
A3SS	505	378
A5SS	624	513
MXE	9	7
RI	1,016	583
SE	381	352
Composite	1,547	1,332
Total	4,082	2,771

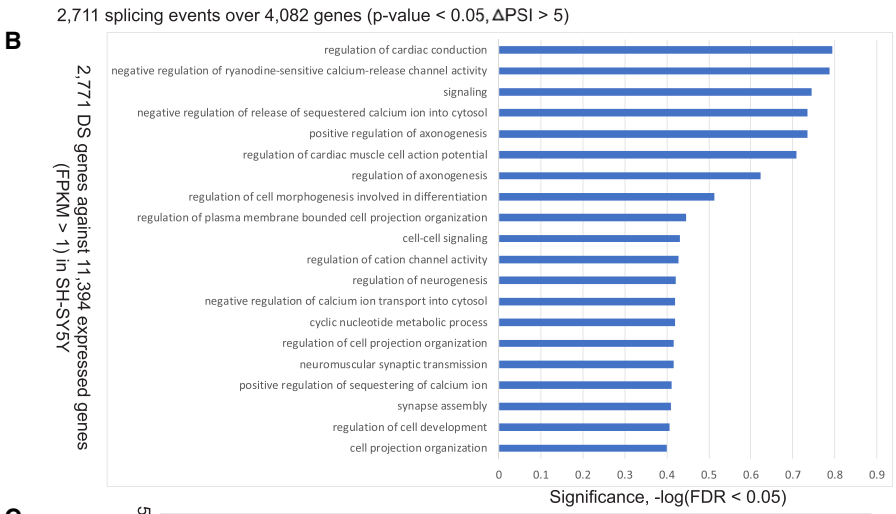

Figure 4. Differential splicing events detected in differentiated neurons derived from homozygous genome-edited SH-SY5Y cells expressing the ALS-associated hnRNPA1 D262V mutation. (*A*) Differential alternative splicing (AS) events detected after differentiation of the SH-SY5Y cells expressing the homozygous ALS-associated hnRNPA1 D262V mutation. Over 2700 splicing events were significantly altered in the hnRNPA1 D262V samples from differentiated neuron cell lines versus wild-type differentiated control cells ($P < 0.05$, $\Delta PSI > 5$). The number of differential splicing events is shown on the *Y*-axis, and the difference in percentage spliced in (PSI) is shown on the *X*-axis. The splicing events were filtered based on the ΔPSI. Types of splicing patterns are indicated at the *right*. Note the dramatic increase in intron retention events. (*B*) A graph of gene ontology (GO) term enrichment of differentially spliced transcripts in differentiated neurons derived from the homozygous hnRNPA1 D262V mutant-expressing SH-SY5Y cells. These groupings correspond to 3322 genes whose splicing pattern is altered in the mutant cells. (*C*) A graph of gene ontology (GO) term enrichment of differentially spliced, intron-retained transcripts in differentiated neurons derived from the hnRNPA1 D262V mutant-expressing SH-SY5Y cells. These groupings correspond to 583 genes whose intron retention splicing pattern is altered in the mutant neurons.

structures, but the chronic stresses associated with aging lead to chronic and persistent SGs that appear to initiate and foster the aggregation of disease-related proteins (Marcelo et al. 2021).

To examine whether there is a difference in stress granule formation under stress in hnRNPA1 D262V mutant-expressing SH-SY5Y cells, we treated the neuronal cell line expressing either wild type or the D262V mutant with arsenite to induce stress granules for 30 min and then followed SG assembly and disassembly by immunofluorescence using an eIF3α antibody, a reliable SG marker. In order to observe whether there is any difference in SG disassembly between hnRNPA1 wild-type and D262V mutant cell lines, we also followed SG disassembly for 2 h after removal of arsenite. The majority of hnRNPA1 proteins in the D262V mutant-expressing cells remained in the nucleus with or without arsenite treatment (Supplemental Fig. S9A). Not only did we observe an elevated level of endogenously expressed hnRNPA1 D262V in SH-SY5Y cells, we also found higher numbers of eIF3α-containing speckles in the homozygous D262V mutant hnRNPA1-expressing cells compared with the unedited wild-type controls under normal conditions (Supplemental Fig. S9B). Most importantly, we observed a marked delay in SG disassembly in the hnRNPA1 D262V mutant cell line 2 h after removal of sodium arsenite compared with wild-type cells, as evidenced by the continued presence of SG speckles (Supplemental Fig. 9B). Delayed SG disassembly was also observed using overexpression of two ALS-associated hnRNPA1 mutants, P288A and D262V, in HeLa cells (Beijer et al. 2021). Together, these data indicate differences in RNA metabolism related to stress granule kinetics in hnRNPA1 D262V mutant-expressing cells compared with the wild type.

Interestingly, we were able to identify many transcripts encoding stress granule-associated proteins that were differentially spliced in both neuroblastoma SH-SY5Y and Tet-inducible 293 cells (Supplemental Fig. S10), including transcripts encoding RNA-binding proteins that have been implicated in neurodegenerative disease and proteins shown to associate with other RBPs causative for ALS, such as FUS and TDP-43. These differentially spliced transcripts are encoded by genes whose products were associated with neuronal RNP granules, eIF4A, and SGs (Supplemental Fig. S10).

Analysis and comparison of in vivo RNA binding by wild-type and D262V hnRNPA1 using irCLIP

The expression of the hnRNPA1 D262V mutant protein resulted in alternative splicing changes in thousands of transcripts. We wanted to determine whether the hnRNPA1 D262V mutant protein might bind to a different subset of, or at different locations on, transcripts compared with the wild-type hnRNPA1 protein. A common method for probing RNA–protein interactions in vivo involves UV cross-linking and immunoprecipitation (CLIP) assays, which can be combined with high-throughput sequencing to generate transcriptome-wide binding maps of RNA-binding proteins (Darnell 2010; Hafner et al. 2010; Huppertz et al. 2014; Van Nostrand et al. 2016; Zarnegar et al. 2016). We used one of the latest CLIP methods, called Quick irCLIP, that incorporates an infrared biotinylated adapter for the detection of protein–RNA interactions (Kaczynski et al. 2019). We performed irCLIP experiments using both inducible FLP-In-293 cells expressing hnRNPA1 wild-type or D262V mutant epitope-tagged proteins and SH-SY5Y cells endogenously expressing hnRNPA1 wild-type or the D262V-edited mutant.

We first optimized immunoprecipitation conditions for the hnRNPA1 protein from extracts derived from each cell line. Immunoblot analysis showed efficient recovery of the protein (Supplemental Fig. S11A). Infrared scans of the nitrocellulose-bound immunoprecipitates using FLAG antibody against exogenously expressed epitope-tagged hnRNPA1 wild-type and D262V mutant FLP-In-293 cells are shown in Supplemental Figure S11B, indicating efficient ligation of the biotinylated adapter to the RNA in the hnRNPA1 immunoprecipitates. For the SH-SY5Y cell lines, an anti-hnRNPA1 antibody was used to immunoprecipitate hnRNPA1 from the unedited wild-type or endogenously edited hnRNPA1 D262V mutant cell line extracts (Supplemental Fig. S11D).

After removing PCR duplicates, read mapping, and peak calling, we detected >480,000–580,000 clusters with at least 10 overlapping sequence reads after FDR filtering (FDR P-value < 0.05) for each sample, which mapped to ~8000 genes (Fig. 5A). Next, we compared the differentially spliced target RNAs from our RNA-seq analyses with the transcriptome binding sites of the hnRNPA1 wild-type and D262V mutant proteins in the neuronal cell lines. Approximately 65% of the differentially spliced transcripts were bound by either the hnRNPA1 wild-type or D262V mutant proteins (Fig. 5B). These differentially spliced transcripts correspond to only ~40% of the hnRNPA1 binding target RNAs determined by irCLIP. The majority of observed RNA binding targets between the hnRNPA1 wild-type and D262V mutant proteins were shared (92%–97%), though we did detect 638 transcripts that are uniquely bound by the hnRNPA1 wild-type protein and 272 transcripts genes that are bound to the hnRNPA1 D262V mutant protein in SH-SY5Y cells (Fig. 5B). For the 7567 common genes to which hnRNPA1 wild-type and D262V mutant proteins bind, the hnRNPA1 wild-type and D262V mutant proteins do share the majority of the binding sites on a given transcript, yet we also found unique binding site clusters (57,986) to which only the D262V mutant protein binds that are not bound by the wild-type hnRNPA1 protein. We also showed that the hnRNPA1 D262V mutant protein shares the majority of splicing target pre-mRNAs compared with the wild-type hnRNPA1 protein while binding to distinct sites on the transcripts using irCLIP in vivo binding assays for hnRNPA1 D262V protein in SH-SY5Y cells. Enrichment motif analysis of irCLIP binding clusters found similar logos that resembled the hnRNPA1 in vitro SELEX binding motif (Burd and Dreyfuss 1994) for both wild-type and D262V mutant hnRNPA1 proteins (Fig. 5C). This observation may not be too surprising, since the disease-associated hnRNPA1 mutation resides within the

A

	Total reads	Clusters with at least overlapping >10 reads	Clusters after FDR filtering, p-value < 0.05	Genes
Flp-In hnRNPA1 WT	43,275,972	3,545,811	519,183	8,075
Flp-In hnRNPA1 D262V	42,284,882	3,940,801	483,849	8,012
SH-SY5Y hnRNPA1 WT	53,554,510	3,690,076	583,264	8,205
SH-SY5Y hnRNPA1 D262V	48,900,645	3,357,153	539,011	7,839

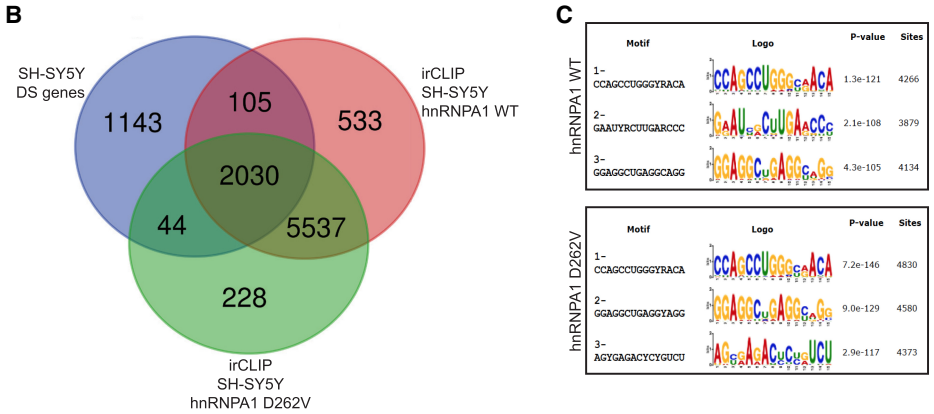

Figure 5. Transcriptome-wide irCLIP binding maps of hnRNPA1 wild-type and D262V mutant proteins. (*A*) A summary of irCLIP-seq data performed in FLP-In-293 and SH-SY5Y cells expressing the hnRNPA1 wild-type and D262V mutant proteins. (*B*) Venn diagram showing the overlap between the differential splicing target RNAs from mutant SH-SY5Y cells (blue) and transcriptome binding sites of hnRNPA1 wild-type (red) and D262V mutant (green) proteins in SH-SY5Y cells. (C) RNA sequence motifs derived from the hnRNPA1 wild-type and D262V binding clusters that were generated by extracting k-mers from read clusters after comparison with control data sets with reads randomly distributed over the same genomic features (see the Materials and Methods).

low-complexity domain and not within RNA binding RRM domains. There is biochemical evidence that the C-terminal low-complexity domain of hnRNPA1 mediates protein–protein interactions (Cartegni et al. 1996; Jean-Philippe et al. 2013).

Importantly, a comparison of RNA-seq data from SH-SY5Y hnRNPA1 wild-type and D262V mutant cells indicates that there are splicing changes associated with differential hnRNPA1 protein binding. JUM analysis revealed that *DNAJC7* gene transcripts are alternatively spliced in an intron retention (IR) mode. A recent study described how exome sequencing in amyotrophic lateral sclerosis patients implicated a novel gene, DNAJC7, encoding a heat shock protein (Farhan et al. 2019). We observed an intron retention event for transcripts from the DNAJC7 gene in hnRNPA1 D262V mutant-expressing cells (Fig. 6). This intron retention event could trigger nonsense-mediated mRNA decay (NMD). While the hnRNPA1 wild-type and D262V mutant proteins mostly share common binding sites on the DNAJC7 transcript, only hnRNPA1 wild-type binding is observed at the upstream exon junction region (Fig. 6A, indicated in blue). This lack of exon junction binding by the D262V mutant protein could lead to the intron retention events observed in hnRNPA1 D262V mutant-expressing cells compared with the wild-type SH-SY5Y cells. Notably, the mutant D262V mutant protein has new CLIP tags within the intron, which might also contribute to intron retention observed in the DNAJC7 transcript (Fig. 6A, indicated in red). We determined whether the DNAJC7 protein is down-regulated in the Cas9-edited SH-SY5Y cells expressing the hnRNPA1 D262V protein by immunoblot analysis. We found that DNAJC7 goes into insoluble material using mild lysis buffer (0.5% n-dodecyl-b-D-maltoside, 150 mM NaCl, 50 mM HEPES-NaOH at pH 7.4) only in hnRNPA1 D262V mutant samples, just like the GLS protein shown in Supplemental Figure S3. We did observe a smaller molecular weight species only in the hnRNPA1 D262V samples in mild lysis buffer (below the quantified band in Fig. 6B, top panel) that was detected using the DNAJC7 antibody. n-dodecyl-D-maltoside, which is used in the mild lysis buffer, is especially useful for solubilizing membrane proteins to preserve their activity. We do not know whether this band is a truncated form of DNAJC7. We observed similar DNAJC7 protein levels in hnRNPA1 D262V cells compared with the wild-type samples in strong lysis buffer containing 2% SDS (Fig. 6B, bottom panel) and without detection of lower-molecular-weight species that were detected in D262V samples with mild lysis buffer.

Several more detailed examples of hnRNPA1 wild-type and D262V mutant protein binding to differentially spliced transcripts are shown in Supplemental Figures S12 and S13. In each case, altered protein binding is

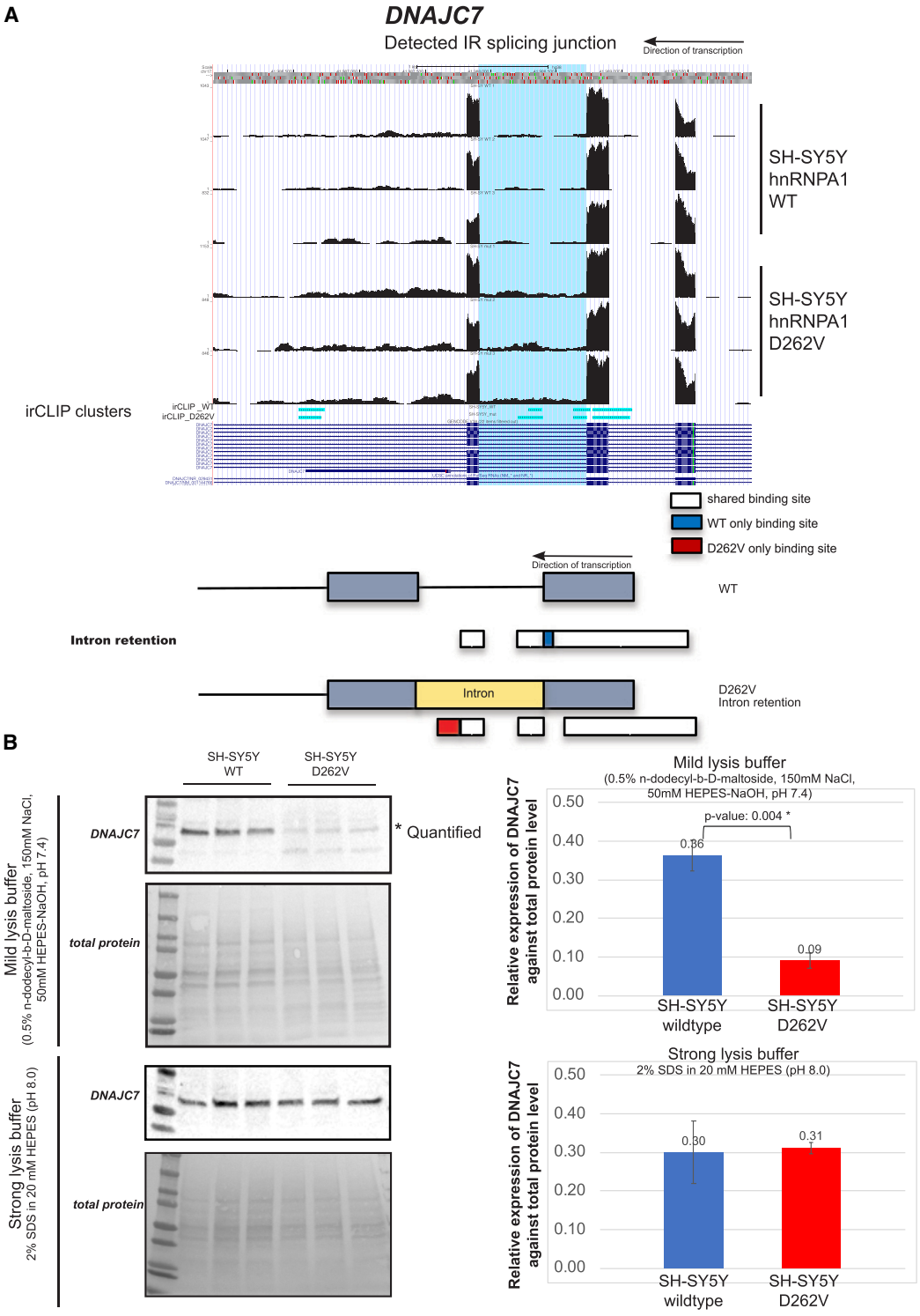

Figure 6. An example of intron retention in *DNAJC7* transcripts in hnRNPA1 D262V mutant-expressing SH-SY5Y cells. (*A*) *DNAJC7* is a protein-folding chaperone and a newly discovered gene implicated in amyotrophic lateral sclerosis. An intron retention event is observed for the *DNAJC7* transcripts in hnRNPA1 D262V mutant-expressing cells, possibly triggering nonsense-mediated (NMD) mRNA decay that would lead to down-regulation of the *DNAJC7* mRNA and protein. *Below*, there is loss of wild-type hnRNPA1 irCLIP tags near the intron–exon border and a gain of intronic D262V hnRNPA1 irCLIP tags in the retained intron. (*B*). Immunoblot analysis indicates that there is a solubility difference between hnRNPA1 wild-type and hnRNPA1 D262V mutant protein samples in mild lysis buffer. DNAJC7 protein goes into the insoluble fraction in mild lysis buffer. Total protein expression was used as a loading control. Normalized relative expression of DNAJC7 is shown in the graph. Bars indicates standard deviation. $N = 3$. Significance in difference between the two groups was tested by Student's *t*-test (P-value = 0.004).

correlated with a change in the pre-mRNA splicing pattern. In many cases, as with DNAJC7, there are new binding sites for the hnRNPA1 D262V mutant protein, suggesting that even though the D262V mutation lies outside the RNA-binding domains of hnRNPA1, it can still affect where the protein binds to target pre-mRNAs.

Proteomic analysis of hnRNPA1 wild-type and D262V mutant proteins

We next wanted to investigate the idea that the hnRNPA1 D262V mutant protein, which exhibits an aggregation phenotype at high concentrations in vitro compared with wild type (Kim et al. 2013), might alter protein–protein interactions in vivo. Tandem mass tag mass spectrometry (TMT-MS/MS), which enables identification and quantitation of proteins in different samples, was used to make a direct comparison of protein–protein interactions detected with wild-type and mutant hnRNPA1. Isobaric labeling via tandem mass tag (TMT) reagents enabled sample multiplexing prior to LC–MS/MS, facilitating high-throughput large-scale quantitative proteomics. First, we again optimized immunoprecipitation conditions to completely deplete hnRNPA1 proteins from SH-SY5Y cell extracts expressing either the hnRNPA1 wild-type or D262V mutant proteins (Supplemental Fig. S14A). Immunoprecipitation was performed in triplicate on either wild-type or homozygous D262V mutant-expressing SH-SY5Y cells, the cells were proteolyzed, mass tags were added, and then the cells were subjected to LC-MS/MS (without RNase treatment: two independent TMT-MS/MS runs and four immunoprecipitated samples from wild-type and D262V mutant-expressing cells; with RNase treatment: one TMT-MS/MS run and three immunoprecipitated samples from wild-type and homozygous D262V mutant-expressing SH-SY5Y cells). Normalized average intensity values were used for quantitation from the TMT-MS/MS results to generate a heat map (Fig. 7).

Coimmunoprecipitation experiments with or without RNase treatment were used to validate a few of the interaction partners of the hnRNPA1 wild-type and D262V mutant proteins and to distinguish between direct and indirect interactions (Supplemental Figs. S14B, S15). Cells were treated either with or without RNase after incubation with the lysate, and bound immunoprecipitates were subjected to immunoblot analysis. This analysis indicated that many interactions required RNA to be detected, indicating that the proteins might be bound to RNAs with which hnRNPA1 stably interacted but not necessarily by direct protein–protein interactions. We were able to validate a subset of hnRNPA1-interacting proteins from a large mass spectrometry list that included a few known hnRNPA1 interactors (hnRNP L, hnRNP H, and ILF3) as well as novel hnRNPA1 interactors (PHB and PHB2). We were particularly interested in PHB (prohibitin 1), as PHB was one of the most abundant proteins in the hnRNPA1 immunoprecipitates based on normalized average intensity values. PHB is involved in cellular senescence. Together with PHB2, the prohibitin complex plays a role in the mitophagy receptor involved in targeting mitochondria for autophagic degradation (Wei et al. 2017). It will be interesting to further characterize the PHB protein interaction with mutant hnRNPA1, as this could alter autophagic degradation in D262V-expressing cells.

A comprehensive analysis of the TMT mass spectrometry data indicates that there were hundreds of differential protein–protein interactions detected between the hnRNPA1 wild-type and D262V mutant proteins in cells (a subset of the TMT-MS/MS list is shown in Fig. 7; Supplemental Table S1). We detected 200 proteins that showed increased interaction with the D262V mutant protein. The genes encoding these proteins included chaperonin, heat shock proteins, peptidylprolyl isomerase a, calnexin, prostaglandin E synthase 3, and proteasome. These genes are involved in cellular processes such as protein folding, neutrophil degranulation, and regulated exocytosis (Supplemental Fig. 16A). We also identified 100 proteins that exhibit a decreased interaction with the D262V mutant protein (Supplemental Table S1). The majority of these proteins were ribosomal proteins and RNA-binding proteins. The GO term enrichment analysis on 100 proteins with a decreased interaction with D262V mutant protein compared with wild type showed that they are involved in SRP-dependent cotranslational protein targeting to membrane and mRNA metabolic process. RNA-binding proteins such as DHX9, RBMX, PABPC1, HNRNPU, DDX17, RPS6, SFPQ, U2AF2, HNRNPA2B1, HNRNPA1, HNRNPF, HNRNPH1, KIAA1429, and YBX1 are listed in this GO term enrichment category, which includes proteins involved in alternative splicing or R-loop formation and protein synthesis (Supplemental Fig. 16B).

We also compared all differential interactome candidates pulled down from our multiple TMT-MS/MS experiments with publicly available data on the Harmonizome database (Rouillard et al. 2016) for hnRNPA1 curated interactors. We identified 101 targets that showed up in our multiple TMT-MS/MS runs and overlapped with known hnRNPA1-interacting proteins on the Harmonizome database (Supplemental Fig. S17). This included known hnRNPA1 interactors, such as hnRNP H, hnRNP L, and ILF3, but also matched our novel hnRNPA1 interactors, such as PHB, BCLAF1, COPA, PRDX1, and DHX9. Many of these were known splicing factors or proteins involved in translational control, mRNA stabilization, and SRP-dependent cotranslational protein targeting to membranes. A decreased interaction between the D262V mutant protein and other RNA-binding proteins involved in alternative splicing could result in altered splicing patterns for thousands of transcripts, as evidenced by our alternative splicing RNA-seq data (Figs. 1, 4). Our experiments revealed that most of these interacting proteins require RNA for interaction, as we only detected RNA-independent interaction with the RNA helicase DDX17, serine/threonine-protein phosphatase PGAM5, polyadenylate-binding protein 1 (PABPC1), ribosomal subunits, and cytoskeletal proteins (Supplemental Table S2). This suggests that the C terminus of hnRNPA1 interacts with other proteins bound to pre-mRNA, which could explain how the mutant hnRNPA1 protein can stably bind to new binding sites.

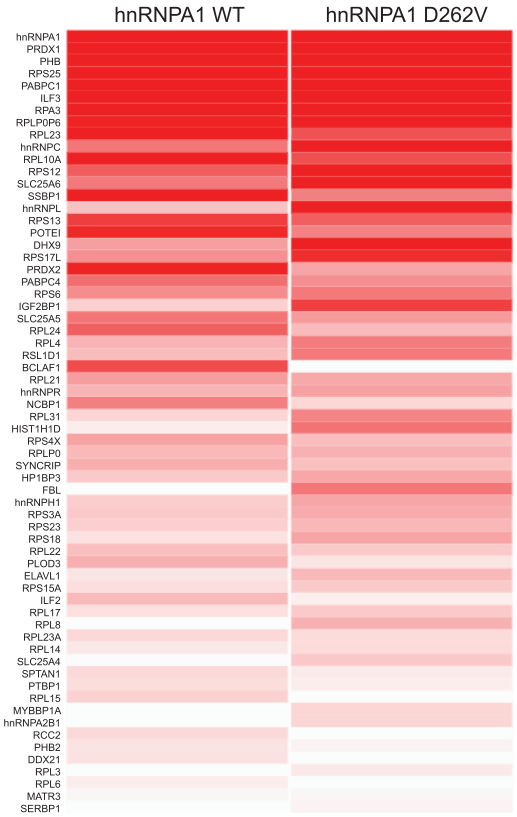

TMT mass spec	SH-SY5Y cells
Interaction only in WT	IGKV2D28, RPL15, RPL6, DDX21, BCLAF1, RCC2
Interaction only in D262V	FBL, hnRNPA2B1, RPL3, RPL8, SERBP1, MYBBP1A
WT > D262V	ILF2, PLOD3, NCBP1, PHB2, PRDX2, RPL23, RPL24, PHB, PTBP1, SSBP1, PRDX1, SPTAN1, POTEI, RPL10A, SLC25A5, RPS4X, PABPC4, SYNCRIP, RPS13, RPL22, RPA3, PABPC1, RPL21, RPL23A
D262V > WT	RPLP0, ILF3, RPS6, hnRNPR, hnRNPA1, RPS23, RPS25, RPS12, RPS3A, HP1BP3, RPLP0P6, RPS15A, RPL4, hnRNPH1, RPL17, RPL14, SLC25A6, RPS17L, RSL1D1, DHX9, hnRNPC, RPL31, ELAVL1, RPS18, IGF2BP1, hnRNP L, HIST1H1D, SLC25A4

Figure 7. Tandem mass tag mass spectrometry (TMT-MS/MS) of differentially interacting proteins in hnRNPA1 wild-type and D262V mutant-expressing SH-SY5Y cells. (*Left*) Heat map of protein/peptide abundance differences between hnRNPA1 wild-type and D262V mutant immunoprecipitated protein samples. Normalized average ion intensity values for quantitation of peptides detected from the indicated proteins using TMT-MS/MS were used for display. (*Right*) A summary of identified proteins found and/or enriched in the different samples is shown.

Discussion

Impaired RNA processing and dysregulation are key features in the development of neurodegenerative diseases, including ALS, by altering RNA metabolism and causing loss of protein homeostasis. Mutations in the low-complexity domains of hnRNPA1 and hnRNPA2B1 account for <1% of familial and sporadic forms of ALS (Taylor et al. 2016; Harley et al. 2021). However, muscle biopsies from patients with multisystem proteinopathy showed cytoplasmic mislocalization and partial colocalization of TDP-43 and hnRNPA1 (or hnRNPA2B1) (Kim et al. 2013), suggesting that hnRNPA1 might play a broader role in the disease. In order to investigate the mechanisms by which the ALS-linked hnRNPA1 D262V mutation might contribute to ALS disease manifestation, we took two different approaches. First, we generated inducible cell lines to express either hnRNPA1 wild-type or D262V mutant cDNAs while expressing endogenous hnRNPA1. Second, we used genome editing with Cas9 at the endogenous hnRNPA1 locus in SH-SY5Y human neuronal cells to generate homozygous hnRNPA1 D262V mutant cell lines. We observed a cell aggregation phenotype in hnRNPA1 D262V mutant cell lines in both FLP-In-293 and SH-SY5Y cells compared with wild type, as well as markedly slower growth and neuronal process and connection defects in D262V mutant neurons.

Our studies showed that expression of the hnRNPA1 D262V mutant protein altered pre-mRNA splicing of thousands of transcripts, and gene ontology (GO) term analysis indicated that the genes whose transcripts are differentially spliced are involved in DNA repair, the cellular response to DNA damage stimuli, chromatin remodeling, and cilium assembly. We also searched our data sets to ask whether transcripts encoding known neurodegenerative disease-associated proteins are differentially spliced in cells expressing hnRNPA1 mutant proteins. These ALS-linked proteins include cytoskeletal proteins, RNA-binding proteins, and proteins involved in translational control and proteostasis. While GO term enrichment analysis of differentially spliced transcripts mainly yielded DNA repair, cilium organization, and response to DNA damage, many known ALS-associated gene transcripts (e.g., TDP-43 and FUS) were shown to be differentially spliced in the hnRNPA1 D262V mutant-expressing cell lines, giving us more confidence that the splicing targets detected by this RNA-seq analysis are relevant to ALS.

Our RNA-seq data in edited SH-SY5Y cells showed a striking difference in the splicing patterns between undifferentiated and differentiated neuronal cells. Mutant

hnRNPA1 D262V differentiated SH-SY5Y cells showed elevated intron retention and composite modes of splicing events compared with the wild-type cells. The intron retention mode of splicing is one of the least commonly observed human splicing patterns. Notably, elevated intron retention was also observed in C9orf72 ALS patient brain biopsy RNA-seq data sets (Wang et al. 2020). Intron retention might lead to nonsense-mediated RNA decay (NMD), which has been linked to neuronal physiology and neurodegeneration (Petric Howe and Patani 2023).

We also have shown that the hnRNPA1 D262V mutant protein shares the majority of splicing target pre-mRNAs compared with the wild-type hnRNPA1 protein, but that the mutant D262V protein binds to distinct sites. While the D262V mutation may not affect RNA binding specificity, protein–protein interactions with other RNA-bound proteins mediated by the C-terminal low-complexity domain of hnRNPA1 may alter the affinity of the mutant protein at some binding sites, leading to differential splicing of the target pre-mRNAs. This idea would explain both the novel irCLIP tags found for the D262V mutant protein and also why the proteomics data indicated that RNA was required to retrieve many of the proteins found in the hnRNPA1 immunoprecipitation.

TDP-43 is known to regulate alternative splicing of hnRNPA1 pre-mRNA to yield a spliced variant that is prone to aggregation in 293 and HeLa cells (Deshaies et al. 2018). Both TDP-43 and hnRNPA1 are well-established splicing regulators, and mutations within their low-complexity domains are associated with neurodegenerative disease. In order to determine whether there is overlap between TDP-43 splicing targets and those of hnRNPA1, we used publicly available TDP-43 knockdown and TDP-43 N352S RNA-seq data sets and performed differential splicing analysis using JUM. Our analysis indicated an ~30%–35% overlap in differentially spliced transcripts between TDP-43 and hnRNPA1. This indicates that although TDP-43 and hnRNPA1 are involved in splicing coregulation and share some common splicing targets, they also clearly have distinct splicing targets from each other.

hnRNPA1 mainly localizes to the nucleus under normal conditions, and it has been shown previously that only a small fraction of hnRNPA1 translocates to cytoplasmic stress granules (SGs) under treatments such as heat shock and sodium arsenite, while the majority of hnRNPA1 remains in the nucleus (Liu et al. 2016; Beijer et al. 2021). We observed a statistically significant delay in SG disassembly in the hnRNPA1 D262V mutant SH-SY5Y mutant cell line compared with the wild type after removal of sodium arsenite. Notably, we also observed elevated cytoplasmic localization of the D262V protein and higher numbers of SG speckles even under normal conditions in the absence of external stimuli, which was not previously observed. Together, these data indicate differences in RNA metabolism in hnRNPA1 D262V mutant-expressing cells compared with wild type. Interestingly, we also identified many transcripts encoding stress granule-associated proteins that were differentially spliced in both cell lines expressing mutant hnRNPA1, which could contribute to altered RNA metabolism due to cellular stress.

The expression of the mutant hnRNPA1 D262V protein resulted in cells that exhibited a cell aggregation phenotype and a markedly slower cell growth rate. Purified hnRNPA1 D262V mutant protein exhibited elevated protein aggregation at high concentrations in vitro (Kim et al. 2013; Liu et al. 2016; Beijer et al. 2021). It is possible that the hnRNPA1 D262V mutant protein may sequester other proteins in cells, such as other hnRNPs and/or ribosomal proteins, an idea supported by our TMT mass spectrometry data. Defects in the function of RNA-binding proteins or translating ribosomes might lead to the observed slow growth phenotype of the hnRNPA1 D262V mutant cells. While there have been numerous studies with in vitro aggregation assays for ALS-associated mutant RNA-binding proteins (Johnson et al. 2009; Kim et al. 2013; Beijer et al. 2021), this is the first example where an ALS-associated mutant in hnRNPA1 has an in vivo phenotype (e.g., slower cell growth) that is clearly different from the wild type. A slower growth defect phenotype was observed in both genome-edited SH-SY5Y cells and in FLP-In-293 cells expressing the inducible hnRNPA1 D262V mutant. When we differentiated SH-SY5 cells for 18 d, we found that the neuronal processes and connections in hnRNPA1 D262V-expressing neuronal cells were fewer and less extensive compared with wild-type cells. This might arise from cytoskeletal or cilium defects in the mutant cells. Cytoskeletal genes were shown to be alternatively spliced in both FLP-In-293 and SH-SY5Y cells expressing hnRNPA1 D262V mutant proteins. GO term enrichment analysis of these differentially spliced transcripts in neuronal cells expressing the hnRNPA1 D262V mutant indicated that these genes were involved in cilium assembly and cell projection assembly. Taken together, these data show that expression of the hnRNPA1 D262V mutant leads to changes in cell–cell contacts, a marked reduction in growth rate, and defective branching out of neuronal processes and connections characteristic of mature neurons.

Our TMT mass spectrometry data indicated that there were hundreds of differential protein–protein associations detected between the hnRNPA1 wild-type and D262V mutant proteins in cells. We detected 200 proteins that showed increased interaction with the D262V mutant protein and 100 proteins that exhibited a decreased interaction. We identified known hnRNPA1 interactors such as hnRNP H, hnRNP L, and ILF3 but also revealed new hnRNPA1 interactors such as PHB, BCLAF1, COPA, PRDX1 and DHX9. We observed a decreased association between the D262V mutant protein and other RNA-binding proteins involved in alternative splicing, which could result in altered splicing patterns for thousands of transcripts. We validated a few of the interacting partners of hnRNPA1 wild type and the D262V mutant by coimmunoprecipitation experiments with or without RNase treatment to distinguish direct or indirect interactions with the hnRNPA1 proteins. It seems many of the proteins that copurified with hnRNPA1 require RNA to be detected, consistent with the idea that the mutant hnRNPA1

protein may bind stably to new sites on target RNAs by interacting with other RNA-binding proteins nearby. Protein–protein interactions between RNA-binding proteins may stabilize binding of both proteins to a target RNA. These interactions would only occur on the RNA and would then be sensitive to RNase treatment in an immunoprecipitation experiment. This idea also fits with our comparison of the in vivo RNA-binding sites for hnRNPA1 D262V mutant and wild-type proteins. Similar binding motifs were found for both the hnRNPA1 wild-type and D262V mutant proteins, but we also observed some differential binding sites for the wild-type and D262V mutant hnRNPA1 proteins that can be correlated with altered splicing patterns of the target transcripts. We showed that binding of the hnRNPA1 D262V mutant to new sites on a transcript correlated with perturbed alternative splicing, thus contributing to the thousands of altered splicing events that we observed in D262V-expressing cells.

Our previous hnRNPA1 knockdown and in vivo RNA binding data indicated that hnRNPA1 can bind thousands of RNA transcripts in cells (Lee et al. 2018). Our new data indicate that the expression of an ALS-causing hnRNPA1 D262V mutant alone can alter splicing patterns of thousands of transcripts involved in DNA damage and repair, primary cilia, and translation. Numerous neurodegenerative diseases have been associated with defects in primary cilia (Ki et al. 2021). A potential link between autophagy dysfunction and a primary cilium defect has been implicated in Huntington's disease (Kaliszewski et al. 2015). Impaired DNA repair and autophagy dysfunction are two of the proposed mechanisms common in neurodegenerative diseases, along with altered RNA metabolism, impaired protein homeostasis, nucleocytoplasmic transport defects, mitochondrial dysfunction, increased oxidative stress, impaired axonal structure, and transport defects.

Taken together, these findings indicate that a single disease-associated mutation in hnRNPA1 has a dominant-negative phenotype and affects many aspects of cellular metabolism, including alternative splicing and altered protein–protein interactions. Previous studies have indicated that hnRNPA1 binding sites can be targeted by antisense oligonucleotides (ASOs) in cells as a treatment for the neurodegenerative disease SMA (spinal muscular atrophy). Identification of hnRNPA1 splicing targets in cells carrying the D262V mutation might also be relevant for transcripts whose splicing is altered in cells carrying other ALS-linked mutations in the RNA-binding proteins FUS, TDP-43, and TIA1 (Vance et al. 2009; Liu et al. 2013; Mackenzie et al. 2017). This study provides new information about how the hnRNPA1 D262V mutation alters RNA processing and protein homeostasis defects leading to ALS.

Materials and methods

Cells and generation of hnRNPA1 D262V cell lines

Human SH-SY5Y cells (American Type Culture Collection) were maintained at 37°C in DMEM/F-12 (Gibco 11320082) medium supplemented with 10% FBS and 1% penicillin/streptomycin. Wild-type and mutant FLAG-tagged hnRNPA1 cDNAs were generated by PCR and cloned into pcDNA4/FRT/TO. Human FLP-In T-REx-293 cell lines (Invitrogen R78007) expressing hnRNPA1 wild-type or D262V mutant cDNAs were generated by cotransfecting the hnRNPA1 cDNAs with a FLP recombinase expression plasmid according to the manufacturer's instructions. Cells were maintained in DMEM (high glucose), 10% FBS, 2 mM L-glutamine, and 1% penicillin/streptomycin. Twenty-thousand SH-SY5Y cells were transfected with 6 µL (180 pmol) of 30 µM sgRNA and 0.5 µL of 20 µM recombinant Cas9 nuclease. After 10 min of incubation at room temperature, RNP complexes were transfected with 1 µL of 100 µM mutant donor oligo. A phosphorothioate-modified DNA oligonucleotide (GGAT CCTACAATGTTTTTGGC) was used as a donor for Cas9-mediated genome editing. A BamHI restriction site was incorporated into the donor oligonucleotide for screening purposes. After transfection, cells were plated to single cells, grown, and screened by genomic PCR. SH-SY5Y cells had to be plated on irradiated mouse embryonic fibroblasts (MEFs) for single-cell cloning. Once edited colonies were identified, the presence of the desired mutation was confirmed by Sanger sequencing of the PCR fragments.

Differentiation of SH-SY5Y cells

SH-SY5Y cells were differentiated accordingly to a published protocol (Shipley et al. 2016) with the following modifications: F12/DMEM media with 10% FBS was used in place of EMEM media with 15% FBS as the basic growth media; 2.5% FBS F12/DMEM with 1× penicillin/streptomycin, 2 mM glutamine, and 10 µM RA was used as differentiation media 1; 1% FBS F12/DMEB with 1× penicillin/streptomycin, 2 mM glutamine, and 10 µM RA was used as differentiation media 2; and F12/DMEM with 1× B-27, 20 mM KCl, 1× penicillin/streptomycin, 2 mM GlutamaxI, 50 ng/mL BDNF, 2 mM dibutyryl cyclic AMP (db-cAMP), and 10 µM RA was used as differentiation media 3. SH-SY5Y cells were differentiated as described previously (Shipley et al. 2016) and harvested on day 18 for imaging experiments and RNA-seq library preparation.

Immunoblotting

Lysates were prepared in RIPA buffer (50 mM Tris-HCl at pH 7.4, 150 mM NaCl, 1% [v/v] Nonidet P-40, 0.5% [w/v] sodium deoxycholate, 0.1% [w/v] sodium dodecyl sulfate [SDS]) containing protease inhibitors, mild lysis buffer used in mass spectrometry (0.5% n-dodecyl-b-D-maltoside, 150 mM NaCl, 50 mM HEPES-NaOH at pH 7.4), or strong lysis buffer (2% SDS, 20 mM HEPES at pH 8.0). Equivalent amounts of each sample were subjected to immunoblotting with the following antibodies: hnRNPA1 (clone 9H10; 1:1000 dilution; Sigma R4528), FLAG (1:1000 dilution; Sigma F3165), β-actin (1:3000 dilution; Sigma A2228), DNAJC7 (1:1000 dilution; Proteintech C860T18), PHB (1:1000 dilution; Proteintech 10787-1-

AP), hnRNP H (1:1000 dilution; Abcam ab10374), ILF3 (1:1000 dilution; Proteintech 19887-1-AP), and DHX9 (1:1000 dilution; Proteintech 17721-1-AP).

Immunofluorescence (IF) assays

Cells (4.5×10^5) were plated 24 h before performing IF. Cells were fixed in 4% paraformaldehyde solution and incubated for 10 min at 37°C, followed by methanol fixation for 10 min. The cells were blocked using 6% BSA for 1 h at room temperature, followed by incubation with primary antibodies for 2–3 h. The cells were washed three times in 1× PBS/0.05% Tween 20 and then incubated with secondary antibodies followed by PBS/0.05% Tween washes. IF was performed using hnRNPA1 (1:500 dilution; Sigma R4528), eIF3α (1:500 dilution; Abcam 3411S), and Alexa fluor 488- or 568-labeled donkey antirabbit or goat antimouse secondary antibodies (1:1500 dilution; Life Technologies A10042 and A11029), and cells were mounted with DAPI-containing VectaShield mounting medium (Vector Laboratories). The images were obtained at the CNR Biological Imaging Facility, University of California, Berkeley.

RNA-seq library preparation and sequencing

RNA isolation was performed using the RNeasy minikit (Qiagen 74104) followed by 30 min of DNase treatment (Ambion AM2238) at 37°C. Poly(A)$^+$ RNA transcripts were isolated [NEBNext poly(A) mRNA magnetic isolation module; New England Biolabs E7490] from 1 µg of total RNA for RNA library preparation and sequencing using the NEBNext ultradirectional RNA library preparation kit for Illumina (New England Biolabs E7420S) according to the manufacturer's instructions. The samples were sequenced on an Illumina HiSeq 4000 (FLP-In-293) NovaSeq SP (SH-SY5Y) with 100-bp paired-end reads at the Vincent J. Coates Genomics Sequencing Laboratory at the University of California, Berkeley. Differentiated SH-SY5Y neuronal cells (18 d) were sequenced on an Illumina NovaSeq S4 with 150-bp paired-end reads at the same facility.

Analysis of pre-mRNA splicing patterns using JUM, and differential expression analysis using DESeq2

Pre-mRNA splicing analysis using JUM 2.0.2 software to detect pre-mRNA splicing patterns was performed as described before (Lee et al. 2018). A *P*-value of 0.05 was used as the statistical cutoff for differentially spliced AS events. Expressed genes for GO term enrichment analysis were generated using Cufflinks v2.1.1 (Trapnell et al. 2009) using the parameter --library-type fr-firststrand -m 100 -s 10 and then filtered for FPKM of >1.

For differential expression analysis, uniquely mapped reads were mapped to hg38 using STAR_2.5.3a_modified version using --outFilterMultimapNmax 1. Read counts were calculated using the HTSeq script htseq-count with the following specification: -s yes -r pos -f. Differential gene expression analysis was performed using DESeq2 (Love et al. 2014) using CPM cutoff. The expression cutoff (CPM) value was determined according to the library size and normalization factors, roughly equal to $10/L$ where L is the minimum library size in millions (Chen et al. 2016).

Quick irCLIP

To identify the RNAs bound by hnRNPA1 wild type versus D262V mutants, we performed quick irCLIP, crosslinking, and inferred immunoprecipitation according to the previously published protocol (Kaczynski et al. 2019) with minor modifications. The library was prepared using SMARTer smRNA-seq kit for Illumina (Takara 635029) according to the manufacturer's instructions. The samples were sequenced on an Illumina NovaSeq S1 with 100-bp paired-end reads at the Vincent J. Coates Genomics Sequencing Laboratory at the University of California, Berkeley.

The quick irCLIP-seq reads were preprocessed prior to mapping using FASTX-Toolkit (http://hannonlab.cshl.edu/fastx_toolkit). Reads were quality-filtered based on quality score (fastq_quality_ filter -q 25 -p 80), and PCR duplicates were collapsed (fastx_collapser). Only uniquely mapped reads were used for further analysis. The reads were mapped to hg38 using STAR using the following parameter: --outFilterMultimapNmax 1 --quantMode TranscriptomeSAM GeneCounts --outReadsUnmapped fastx --outSAMtype BAM SortedByCoordinate. Uniquely mapped reads were filtered and then used for cluster identification using pycrac 1.2.3.0 (Webb et al. 2014). irCLIP clusters were generated using at least 10 overlapping unique cDNA reads generated after removal of PCR duplicates (pyClusterReads.py --cic = 10). pyCalculateFDRs were used to filter out statistically significant clusters over the regions with a read coverage of at least 5 (--min = 10) and FDR of $P < 0.05$. De novo binding motifs for hnRNPA1 wild-type and mutant protein were determined using STREME (Bailey 2021) using the following parameter: streme --verbosity 1 --oc --rna --minw 8 --maxw 15 --pvt 0.05.

Tandem mass tag (TMT) mass spectrometry

The protocol that we used was modified slightly from a previous study (Griesser et al. 2020). Five-hundred micrograms of cell lysate from SH-SY5Y cells was incubated with 50 µg of hnRNPA1 antibody (Sigma R4528) bound to Dynabeads Protein G beads in lysis buffer (0.5% n-dodecyl-b-D-maltoside, 150 mM NaCl, 50 mM HEPES-NaOH at pH 7.4). The beads were washed four times in 0.1%/Triton X-100 in 25 mM HEPES buffer (pH 7.4). The samples were treated with 10 mM DTT to reduce reversibly oxidized cysteines for 45 min at 50°C and then were alkylated with 20 mM iodoacetic acid with shaking at 1000 rpm for 45 min at room temperature. The samples were subjected to SP3 digestion and TMT-labeled exactly as previously described (Griesser et al. 2020).

To detect RNA-independent protein–protein interactions, the protocol that we used was modified slightly from a previous study (Jäger et al. 2011). Five-hundred micrograms of SH-SY5Y cell lysate (lysis buffer: 0.5% NP40, 50 mM Tris-HCl at pH 7.4, 150 mM NaCl, 1 mM EDTA,

protease and phosphatase inhibitors) from wild-type and D262V-expressing cells was treated with 25 U of RNase A (Invitrogen 12091021) for 30 min on ice. RNase-treated lysates were incubated with 50 µg of hnRNPA1 antibody (Sigma R4528) bound to Dynabeads Protein G beads and incubated overnight at 4°C. The samples were treated with 10 mM DTT to reduce reversibly oxidized cysteines for 45 min at 50°C and then were alkylated with 20 mM iodoacetic acid with shaking at 1000 rpm for 45 min at room temperature. The beads were washed four times in the same lysis buffer. The samples were subjected to SP3 digestion and TMT-labeled exactly as previously described (Griesser et al. 2020).

Mass spectrometry was performed at the Vincent J. Coates Proteomics/Mass Spectrometry Laboratory, University of California, Berkeley. Normalized average intensity value quantitations from TMT-MS/MS were visualized using Clustergrammer (Fernandez et al. 2017). Normalized average ion intensity values were quantitated for peptides detected from the indicated proteins using TMT-MS/MS experiments.

Coimmunoprecipitation assay

Five-hundred micrograms of SH-SY5Y WT and mutant lysate (lysis buffer: 0.5% n-dodecyl-b-D-maltoside, 150 mM NaCl, 50 mM HEPES-NaOH at pH 7.4) was used per coimmunoprecipitation experiment. One-hundred microliters of either Dynabeads M-280 sheep antimouse IgG (Life Technologies 11201D) or Dynabeads M-280 sheep antirabbit IgG (Life Technologies 11203D) was washed twice in lysis buffer and then incubated with 10 µL of antibody for 1 h at 4°C. Beads were washed twice with lysis buffer. Five-hundred micrograms of SH-SY5Y WT and mutant lysate was added to each IP sample and rotated for at least 4 h at 4°C. The beads were washed three times in 0.1%/Triton X-100 in 25 mM HEPES-NaOH buffer (pH 7.4). Bound proteins were eluted with 40 µL of 2× Laemmli sample buffer, resolved on 10% SDS-PAGE, and subjected to immunoblotting. For RNase-treated samples, beads were divided 1:2 after incubation with lysate. Fifty percent of the beads were put aside as "no RNase" samples, and the other 50% were treated with 25 U of RNase A (Invitrogen 12091021) for 10 min at 37°C. Bound proteins were eluted with 40 µL of 2× Laemmli sample buffer, resolved on 10% SDS-PAGE, and subjected to immunoblotting.

Data deposition

The data reported here have been deposited in the Gene Expression Omnibus (GEO) database (https://www.ncbi.nlm.nih.gov/geo/query/acc.cgi?acc=GSE252683) with SRA data accession number PRJNA1060694.

Competing interest statement

The authors declare no competing interests.

Acknowledgments

We thank George Ghanim (MRC Laboratory of Molecular Biology, Cambridge, UK) for designing the hnRNPA1 donor oligonucleotide. We thank Dirk Hockemeyer and his laboratory for providing irradiated mouse embryonic fibroblasts (MEFs) to use as feeder cells for the SH-SY5Y cells. We thank Nicholas Ingolia and his laboratory for allowing our laboratory to use their server for data analysis. This work used the Vincent J. Coates Genomics Sequencing Laboratory at the University of California, Berkeley, supported by National Institutes of Health (NIH) S10 Instrumentation grants S10RR025622, S10RR029668, and S10RR027303. This research used the Savio computational cluster resource provided by the Berkeley Research Computing program at the University of California, Berkeley (supported by the University of California, Berkeley, Chancellor, Vice Chancellor for Research, and Chief Information Officer). IF images were taken at the College of Natural Resources Biological Imaging Facility at the University of California, Berkeley, which was supported in part by the NIH S10 program under award number 1S10RR026866-01. This work used the Vincent J. Proteomics/Mass Spectrometry Laboratory at the University of California, Berkeley, supported in part by NIH S10 Instrumentation Grant S10RR025622. We thank Lori Kohlstaedt of the Vincent J. Proteomics/Mass Spectrometry Laboratory at the University of California, Berkeley, for assistance in the analysis of mass spectrometry data. This work was funded by the NIH grants R01 GM097352 and R35 GM118121, awarded to D.C.R.

Author contributions: D.C.R. and Y.J.L. conceived the study. Y.J.L. performed experiments, analyzed the data, and generated the figures. Y.J.L. and D.C.R. wrote the original draft and reviewed and edited the manuscript. D.C.R. obtained funding.

References

Agholme L, Lindström T, Kågedal K, Marcusson J, Hallbeck M. 2010. An in vitro model for neuroscience: differentiation of SH-SY5Y cells into cells with morphological and biochemical characteristics of mature neurons. *J Alzheimer's Dis* **20:** 1069–1082. doi:10.3233/JAD-2010-091363

Bailey TL. 2021. STREME: accurate and versatile sequence motif discovery. *Bioinformatics* **37:** 2834–2840. doi:10.1093/bioinformatics/btab203

Balendra R, Isaacs AM. 2018. C9orf72-mediated ALS and FTD: multiple pathways to disease. *Nat Rev Neurol* **14:** 544–558. doi:10.1038/s41582-018-0047-2

Beijer D, Kim HJ, Guo L, O'Donovan K, Mademan I, Deconinck T, Van Schil K, Fare CM, Drake LE, Ford AF, et al. 2021. Characterization of HNRNPA1 mutations defines diversity in pathogenic mechanisms and clinical presentation. *JCI Insight* **6:** e148363. doi:10.1172/jci.insight.148363

Burd CG, Dreyfuss G. 1994. Conserved structures and diversity of functions of RNA-binding proteins. *Science* **265:** 615–621. doi:10.1126/science.8036511

Cartegni L, Maconi M, Morandi E, Cobianchi F, Riva S, Biamonti G. 1996. hnRNP A1 selectively interacts through its Gly-rich

domain with different RNA-binding proteins. *J Mol Biol* **259:** 337–348. doi:10.1006/jmbi.1996.0324

Chen S, Sayana P, Zhang X, Le W. 2013. Genetics of amyotrophic lateral sclerosis: an update. *Mol Neurodegener* **8:** 28. doi:10.1186/1750-1326-8-28

Chen Y, Lun AT, Smyth GK. 2016. From reads to genes to pathways: differential expression analysis of RNA-Seq experiments using Rsubread and the edgeR quasi-likelihood pipeline. *F1000Res* **5:** 1438. doi:10.12688/f1000research.8987.2

Conlon EG, Manley JL. 2017. RNA-binding proteins in neurodegeneration: mechanisms in aggregate. *Gene Dev* **31:** 2015–2015. doi:10.1101/gad.308205.117

Cooper-Knock J, Walsh MJ, Higginbottom A, Highley JR, Dickman MJ, Edbauer D, Ince PG, Wharton SB, Wilson SA, Kirby J, et al. 2014. Sequestration of multiple RNA recognition motif-containing proteins by C9orf72 repeat expansions. *Brain* **137:** 2040–2051. doi:10.1093/brain/awu120

Darnell RB. 2010. HITS-CLIP: panoramic views of protein–RNA regulation in living cells. *Wiley Interdiscip Rev RNA* **1:** 266–286. doi:10.1002/wrna.31

DeGeer J, Lamarche-Vane N. 2013. Rho GTPases in neurodegeneration diseases. *Exp Cell Res* **319:** 2384–2394. doi:10.1016/j.yexcr.2013.06.016

Deshaies JE, Shkreta L, Moszczynski AJ, Sidibé H, Semmler S, Fouillen A, Bennett ER, Bekenstein U, Destroismaisons L, Toutant J, et al. 2018. TDP-43 regulates the alternative splicing of hnRNP A1 to yield an aggregation-prone variant in amyotrophic lateral sclerosis. *Brain* **141:** 1320–1333. doi:10.1093/brain/awy062

Dudman J, Qi X. 2020. Stress granule dysregulation in amyotrophic lateral sclerosis. *Front Cell Neurosci* **14:** 598517. doi:10.3389/fncel.2020.598517

Farhan SMK, Howrigan DP, Abbott LE, Klim JR, Topp SD, Byrnes AE, Churchhouse C, Phatnani H, Smith BN, Rampersaud E, et al. 2019. Exome sequencing in amyotrophic lateral sclerosis implicates a novel gene, DNAJC7, encoding a heat-shock protein. *Nat Neurosci* **22:** 1966–1974. doi:10.1038/s41593-019-0530-0

Fernandez NF, Gundersen GW, Rahman A, Grimes ML, Rikova K, Hornbeck P, Ma'ayan A. 2017. Clustergrammer, a web-based heatmap visualization and analysis tool for high-dimensional biological data. *Sci Data* **4:** 170151. doi:10.1038/sdata.2017.151

Gimenez-Cassina A, Lim F, Diaz-Nido J. 2006. Differentiation of a human neuroblastoma into neuron-like cells increases their susceptibility to transduction by herpesviral vectors. *J Neurosci Res* **84:** 755–767. doi:10.1002/jnr.20976

Griesser E, Wyatt H, Ten Have S, Stierstorfer B, Lenter M, Lamond AI. 2020. Quantitative profiling of the human substantia nigra proteome from laser-capture microdissected FFPE tissue. *Mol Cell Proteomics* **19:** 839–851. doi:10.1074/mcp.RA119.001889

Hafner M, Landthaler M, Burger L, Khorshid M, Hausser J, Berninger P, Rothballer A, Ascano M, Jungkamp AC, Munschauer M, et al. 2010. PAR-CliP—a method to identify transcriptome-wide the binding sites of RNA binding proteins. *J Vis Exp* **41:** 2034. doi:10.3791/2034

Hardiman O, Al-Chalabi A, Chio A, Corr EM, Logroscino G, Robberecht W, Shaw PJ, Simmons Z, van den Berg LH. 2017. Amyotrophic lateral sclerosis. *Nat Rev Dis Primers* **3:** 17085. doi:10.1038/nrdp.2017.85

Harley J, Clarke BE, Patani R. 2021. The interplay of RNA binding proteins, oxidative stress and mitochondrial dysfunction in ALS. *Antioxidants* **10:** 552. doi:10.3390/antiox10040552

Huppertz I, Attig J, D'Ambrogio A, Easton LE, Sibley CR, Sugimoto Y, Tajnik M, König J, Ule J. 2014. iCLIP: protein–RNA interactions at nucleotide resolution. *Methods* **65:** 274–287. doi:10.1016/j.ymeth.2013.10.011

Jäger S, Gulbahce N, Cimermancic P, Kane J, He N, Chou S, D'Orso I, Fernandes J, Jang G, Frankel AD, et al. 2011. Purification and characterization of HIV–human protein complexes. *Methods* **53:** 13–19. doi:10.1016/j.ymeth.2010.08.007

Jean-Philippe J, Paz S, Caputi M. 2013. hnRNP A1: the Swiss army knife of gene expression. *Int J Mol Sci* **14:** 18999–19024. doi:10.3390/ijms140918999

Johnson BS, Snead D, Lee JJ, McCaffery JM, Shorter J, Gitler AD. 2009. TDP-43 is intrinsically aggregation-prone, and amyotrophic lateral sclerosis-linked mutations accelerate aggregation and increase toxicity. *J Biol Chem* **284:** 20329–20339. doi:10.1074/jbc.M109.010264

Johnson JO, Pioro EP, Boehringer A, Chia R, Feit H, Renton AE, Pliner HA, Abramzon Y, Marangi G, Winborn BJ, et al. 2014. Mutations in the Matrin 3 gene cause familial amyotrophic lateral sclerosis. *Nat Neurosci* **17:** 664–666. doi:10.1038/nn.3688

Kaczynski T, Hussain A, Farkas M. 2019. Quick-irCLIP: interrogating protein–RNA interactions using a rapid and simple cross-linking and immunoprecipitation technique. *MethodsX* **6:** 1292–1304. doi:10.1016/j.mex.2019.05.014

Kaliszewski M, Knott AB, Bossy-Wetzel E. 2015. Primary cilia and autophagic dysfunction in Huntington's disease. *Cell Death Differ* **22:** 1413–1424. doi:10.1038/cdd.2015.80

Khan SS, Sobu Y, Dhekne HS, Tonelli F, Berndsen K, Alessi DR, Pfeffer SR. 2021. Pathogenic LRRK2 control of primary cilia and Hedgehog signaling in neurons and astrocytes of mouse brain. *Elife* **10:** e67900. doi:10.7554/eLife.67900

Ki SM, Jeong HS, Lee JE. 2021. Primary cilia in glial cells: an oasis in the journey to overcoming neurodegenerative diseases. *Front Neurosci* **15:** 736888. doi:10.3389/fnins.2021.736888

Kim HJ, Kim NC, Wang YD, Scarborough EA, Moore J, Diaz Z, MacLea KS, Freibaum B, Li S, Molliex A, et al. 2013. Mutations in prion-like domains in hnRNPA2B1 and hnRNPA1 cause multisystem proteinopathy and ALS. *Nature* **495:** 467–473. doi:10.1038/nature11922

Kwiatkowski TJ, Bosco DA, LeClerc AL, Tamrazian E, Vanderburg CR, Russ C, Davis A, Gilchrist J, Kasarskis EJ, Munsat T, et al. 2009. Mutations in the *FUS/TLS* gene on chromosome 16 cause familial amyotrophic lateral sclerosis. *Science* **323:** 1205–1208. doi:10.1126/science.1166066

Lee YJ, Wang QQ, Rio DC. 2018. Coordinate regulation of alternative pre-mRNA splicing events by the human RNA chaperone proteins hnRNPA1 and DDX5. *Gene Dev* **32:** 1060–1074. doi:10.1101/gad.316034.118

Le Gall L, Anakor E, Connolly O, Vijayakumar UG, Duddy WJ, Duguez S. 2020. Molecular and cellular mechanisms affected in ALS. *J Pers Med* **10:** 101. doi:10.3390/jpm10030101

Liu YC, Chiang PM, Tsai KJ. 2013. Disease animal models of TDP-43 proteinopathy and their pre-clinical applications. *Int J Mol Sci* **14:** 20079–20111. doi:10.3390/ijms141020079

Liu Q, Shu S, Wang RR, Liu F, Cui B, Guo XN, Lu CX, Li XG, Liu MS, Peng B, et al. 2016. Whole-exome sequencing identifies a missense mutation in *hnRNPA1* in a family with flail arm ALS. *Neurology* **87:** 1763–1769. doi:10.1212/WNL.0000000000003256

Love MI, Huber W, Anders S. 2014. Moderated estimation of fold change and dispersion for RNA-seq data with DESeq2. *Genome Biol* **15:** 550. doi:10.1186/s13059-014-0550-8

Mackenzie IR, Nicholson AM, Sarkar M, Messing J, Purice MD, Pottier C, Annu K, Baker M, Perkerson RB, Kurti A, et al. 2017. TIA1 mutations in amyotrophic lateral sclerosis and

frontotemporal dementia promote phase separation and alter stress granule dynamics. *Neuron* **95:** 808–816.e9. doi:10.1016/j.neuron.2017.07.025

Madabhushi R, Pan L, Tsai LH. 2014. DNA damage and its links to neurodegeneration. *Neuron* **83:** 266–282. doi:10.1016/j.neuron.2014.06.034

Marcelo A, Koppenol R, de Almeida LP, Matos CA, Nóbrega C. 2021. Stress granules, RNA-binding proteins and polyglutamine diseases: too much aggregation? *Cell Death Dis* **12:** 592. doi:10.1038/s41419-021-03873-8

Mejzini R, Flynn LL, Pitout IL, Fletcher S, Wilton SD, Akkari PA. 2019. ALS genetics, mechanisms, and therapeutics: where are we now? *Front Neurosci* **13:** 1310. doi:10.3389/fnins.2019.01310

Milicevic K, Rankovic B, Andjus PR, Bataveljic D, Milovanovic D. 2022. Emerging roles for phase separation of RNA-binding proteins in cellular pathology of ALS. *Front Cell Dev Biol* **10:** 840256. doi:10.3389/fcell.2022.840256

Nussbacher JK, Tabet R, Yeo GW, Lagier-Tourenne C. 2019. Disruption of RNA metabolism in neurological diseases and emerging therapeutic interventions. *Neuron* **102:** 294–320. doi:10.1016/j.neuron.2019.03.014

Påhlman S, Ruusala AI, Abrahamsson L, Mattsson ME, Esscher T. 1984. Retinoic acid-induced differentiation of cultured human neuroblastoma cells: a comparison with phorbolester-induced differentiation. *Cell Differ* **14:** 135–144. doi:10.1016/0045-6039(84)90038-1

Petric Howe M, Patani R. 2023. Nonsense-mediated mRNA decay in neuronal physiology and neurodegeneration. *Trends Neurosci* **46:**879–892. doi:10.1016/j.tins.2023.07.001

Rouillard AD, Gundersen GW, Fernandez NF, Wang Z, Monteiro CD, McDermott MG, Ma'ayan A. 2016. The harmonizome: a collection of processed datasets gathered to serve and mine knowledge about genes and proteins. *Database* **2016:** baw100. doi:10.1093/database/baw1100

Shipley MM, Mangold CA, Szpara ML. 2016. Differentiation of the SH-SY5Y human neuroblastoma cell line. *J Vis Exp* **108:** 53193. doi:10.3791/53193

Sivakumar P, De Giorgio F, Ule AM, Neeves J, Nair RR, Bentham M, Birsa N, Humphrey J, Plagnol V, Acevedo-Arozena A, et al. 2018. TDP-43 mutations increase HNRNP A1-7B through gain of splicing function. *Brain* **141:** e83. doi:10.1093/brain/awy260

Stankiewicz TR, Linseman DA. 2014. Rho family GTPases: key players in neuronal development, neuronal survival, and neurodegeneration. *Front Cell Neurosci* **8:** 314. doi:10.3389/fncel.2014.00314

Taylor JP, Brown RH Jr., Cleveland DW. 2016. Decoding ALS: from genes to mechanism. *Nature* **539:** 197–206. doi:10.1038/nature20413

Trapnell C, Pachter L, Salzberg SL. 2009. TopHat: discovering splice junctions with RNA-seq. *Bioinformatics* **25:** 1105–1111. doi:10.1093/bioinformatics/btp120

Van Nostrand EL, Pratt GA, Shishkin AA, Gelboin-Burkhart C, Fang MY, Sundararaman B, Blue SM, Nguyen TB, Surka C, Elkins K, et al. 2016. Robust transcriptome-wide discovery of RNA-binding protein binding sites with enhanced CLIP (eCLIP). *Nat Methods* **13:** 508–514. doi:10.1038/nmeth.3810

Vance C, Rogelj B, Hortobágyi T, De Vos KJ, Nishimura AL, Sreedharan J, Hu X, Smith B, Ruddy D, Wright P, et al. 2009. Mutations in FUS, an RNA processing protein, cause familial amyotrophic lateral sclerosis type 6. *Science* **323:** 1208–1211. doi:10.1126/science.1165942

Wang Q, Rio DC. 2018. JUM is a computational method for comprehensive annotation-free analysis of alternative pre-mRNA splicing patterns. *Proc Natl Acad Sci* **115:** E8181–E8190. doi:10.1073/pnas.1806018115

Wang Q, Conlon EG, Manley JL, Rio DC. 2020. Widespread intron retention impairs protein homeostasis in C9orf72 ALS brains. *Genome Res* **30:** 1705–1715. doi:10.1101/gr.265298.120

Wang H, Kodavati M, Britz GW, Hegde ML. 2021. DNA damage and repair deficiency in ALS/FTD-associated neurodegeneration: from molecular mechanisms to therapeutic implication. *Front Mol Neurosci* **14:** 784361. doi:10.3389/fnmol.2021.784361

Webb S, Hector RD, Kudla G, Granneman S. 2014. PAR-CLIP data indicate that Nrd1–Nab3-dependent transcription termination regulates expression of hundreds of protein coding genes in yeast. *Genome Biol* **15:** R8. doi:10.1186/gb-2014-15-1-r8

Wei Y, Chiang WC, Sumpter R Jr., Mishra P, Levine B. 2017. Prohibitin 2 is an inner mitochondrial membrane mitophagy receptor. *Cell* **168:** 224–238.e10. doi:10.1016/j.cell.2016.11.042

Wolozin B, Ivanov P. 2019. Stress granules and neurodegeneration. *Nat Rev Neurosci* **20:** 649–666. doi:10.1038/s41583-019-0222-5

Xie H-R, Hu L-S, Li G-Y. 2010. SH-SY5Y human neuroblastoma cell line: in vitro cell model of dopaminergic neurons in Parkinson's disease. *Chin Med J* **123:** 1086–1092.

Zarnegar BJ, Flynn RA, Shen Y, Do BT, Chang HY, Khavari PA. 2016. irCLIP platform for efficient characterization of protein-RNA interactions. *Nat Methods* **13:** 489–492. doi:10.1038/nmeth.3840